CHAOS IN GENERAL RELATIVITY:

SPINNING PARTICLE ORBITS

by

Christopher Verhaaren

A senior thesis submitted to the faculty of

Brigham Young University

in partial fulfillment of the requirements for the degree of

Bachelor of Science

Department of Physics and Astronomy

Brigham Young University

April 2009

BRIGHAM YOUNG UNIVERSITY

DEPARTMENT APPROVAL

of a senior thesis submitted by

Christopher Verhaaren

This thesis has been reviewed by the research advisor, research coordinator, and department chair and has been found to be satisfactory.

Date	Eric Hirschmann, Advisor
Date	Eric Hintz, Research Coordinator
Date	Ross Spencer, Chair

ABSTRACT

CHAOS IN GENERAL RELATIVITY:

SPINNING PARTICLE ORBITS

Christopher Verhaaren

Department of Physics and Astronomy

Bachelor of Science

We examine the question of chaotic particle orbits in general relativity. In particular we consider the dynamics of a spinning test particle in a black hole spacetime. We describe the model of a spinning test particle in general relativity and determine whether or not an orbit is chaotic. For chaotic orbits we calculate the Lyapunov exponent and give an improved method of comparing the exponents of different orbits. We find a class of orbits that are chaotic for physical spin values. We also find new lower bounds on the spin required for more general orbits to be chaotic.

ACKNOWLEDGMENTS

First, I want to thank my wife Hilary for supporting me through research and writing. I would also like to thank Dr. Hirschmann for teaching me relativity and guiding my research and Dr. Nielsen for introducing me to chaos in general relativity. I'd also like to thank Dr. Hirschmann, Dr. Hart, and Dr. Moody for going over my writing.

Contents

List of Figures

Chapter 1

Introduction

Mankind has always watched the movement of bodies in the sky. From dividing the day by way of the sun, to dividing the months by way of the moon, the regularity of celestial motion became foundational to the contexts of life. Throughout history we have become more adept at understanding this motion. Kepler's laws explained the shape and behavior of planetary orbits. His work made our understanding of the regularity of planetary motion more precise. Newton's laws were the next step, governing almost every behavior observed in the heavens from a set of basic principles. By continued analysis of these principles the rich variety of celestial motion was discovered.

One triumph of Newton's law of gravity is the so-called two body problem. The solution of the two body problem determines the motion of two massive bodies connected by gravitational interaction. This solution models the orbit of any planet around the sun when neglecting all other planets. The success of the two body problem comes from its accurate predictions of the planetary motion we observe.

A simplification of the two body problem is the one body problem. The one body problem seeks to find the orbital behavior of a test particle or, a particle so

much less massive than the body it orbits that we neglect any effects due to its mass. The exact solutions to both the one and two body systems allow a straightforward categorization of all their orbital behavior. The typical categorization relates the energy of the system, whether negative, zero, or positive, to the shape of the orbit. Respectively, these orbital shapes are elliptical, parabolic, and hyperbolic.

In contrast with the simple solutions to the one and two body problems, the three body problem has eluded a general solution for well over three hundred years. In 1887 Henri Poincaré showed that when Newton's gravity describes the motion of three massive bodies our ability to predict their motion becomes very limited. In order to predict the behavior of this system we would need to know the initial conditions exactly. Poincaré's work was among the first to introduce some of the foundational ideas of what is now called chaos theory.

In 1915 Einstein advanced our understanding of gravity by publishing his general theory of relativity. This theory of gravity improves experimental predictions at the cost of some Newtonian assumptions. As opposed to the Newtonian definitions of absolute space and absolute time, relativity reveals space and time as intimately woven together. This union of space and time, called spacetime, acts as the stage upon which physical phenomena take place.

The cornerstone idea of general relativity is that the geometry of spacetime dictates the motion of matter in the universe, and that the distribution of matter defines the geometry of spacetime. These physical ideas require the more sophisticated mathematics of differential geometry to extract physical consequences from the theory. Still, mathematical difficulties aside, general relativity makes predictions beyond the scope of Newton's theory.

These predictions of general relativity have added to our understanding of the heavens and how to study them. Relativity predicts the bending of light by massive

objects and gives a more accurate value of Mercury's perihelion precession. General relativity has also introduced us to black holes and other behavior strange to our Newtonian intuition. These new predictions have been experimentally supported, but come at the price of a much more complicated theory.

The orbits predicted by general relativity reflect this complication. Compared to Newtonian mechanics, where the one and two body problems have similarly simple solutions, in general relativity the two body problem is much more difficult than the one body case.

The complexity of relativity can also be seen in the catalogue of different orbital types. Recall that all one body Newtonian orbits belong to one of three categories. In general relativity one body orbits need a "periodic table" to categorize the possibilities [1]. This increase in variety results from general relativity's relative complexity to Newtonian gravity.

One aspect of this increased complexity are chaotic orbits. In the Newtonian case chaotic orbits first become possible in the three body problem, but this need not be the case for relativity.

Similar to the Newtonian case, the typical one body problem in relativity is guaranteed not to be chaotic. This guarantee can be removed however, by slightly altering the system to model a spinning test particle. Numerical modeling has shown that spinning test particles can produce chaotic orbits when the central mass is stationary [2] and when it is rotating [3, 4].

While these chaotic orbits can be numerically simulated, many are not physically realizable. These orbital types require the test particle to spin much more than is physically possible before the orbit becomes chaotic. Comparing the numerical results to current theoretical bounds on the spin of astrophysical bodies [3] seems to imply that no physical systems of this type are chaotic. Still, due to the variety of possible

orbits, chaotic orbits cannot be ruled out completely.

Since many astrophysical systems we observe fit the spinning test particle approximation, physical chaotic orbits are of some interest. Gravitational wave detection may also be affected by chaotic orbits. Extreme mass binaries, two body systems in which one mass is a black hole that is much larger than the other mass, fit the test particle approximation and are likely sources for detectable gravitational waves. The gravitational radiation emitted from a chaotic source appears to be random. So, if the orbiting binary is chaotic, it will be difficult to separate the gravitational wave signal from noise [5–7]. Numerical modeling of this chaotic behavior may lead to better methods of detecting chaotic signals.

We focus on a spinning particle in the Schwarzschild spacetime similar to [2],while using a more correct method for quantifying the chaos of a given orbit. This method was employed in [3], but we use different criteria to compare one orbit with another. This new method of comparison shows chaotic orbits undiscovered by [2] and [3]. We analyze these unexamined chaotic orbits which allows us to set a new lower bound on the spin required for chaos in the Schwarzschild spacetime.

Chapter 2

Orbits in General Relativity

Test particle orbits are some of the simplest physical systems modeled by general relativity that have nontrivial behavior. We use these nonspinning particle orbits as a basis for our understanding of spinning particles.

In general relativity gravity is not seen as a force but a consequence of the geometry of spacetime. In order make calculations of the physical consequences of this theory we need the mathematics of differential geometry. We will briefly introduce some of these concepts and refer the reader of an introductory text on general relativity for a more complete treatment.

The defining quality of a spacetime is its metric. The metric, denoted g_{ab}, defines notions of distance and angle in the spacetime and is independant of the coordinates used to map the spacetime. For example suppose the spacetime was a three dimensional Euclidean space $\mathbb{R}^3$. Then if we pick cartesian coordinates the distance is defined by the Pythagorean theorem. We can then define the metric in two equivalent ways. The first is the line element

$$ds^2 = dx^2 + dy^2 + dz^2 \tag{2.1}$$

which defines the differential definition of distance. The second representation of the

metric is a symmetric $n \times n$ matrix where n is the dimension of the space. So in $\mathbb{R}^3$ we have

$$g_{ab} = \begin{pmatrix} 1 & 0 & 0 \\ 0 & 1 & 0 \\ 0 & 0 & 1 \end{pmatrix} \tag{2.2}$$

Notice how the line element corresponds to the matrix representation. The line element has no cross terms, such as $dxdy$, and the matrix has no off-diagonal elements. Since matrix computations with diagonal matrices is fairly simple it is often desirable to pick coordinates that make the metric diagonal if possible. As a second example, the line element and matrix representation for Minkowski space, the arena of special relativity, are

$$ds^2 = dt^2 - dx^2 - dy^2 - dz^2 \tag{2.3}$$

and

$$\eta_{ab} = \begin{pmatrix} 1 & 0 & 0 & 0 \\ 0 & -1 & 0 & 0 \\ 0 & 0 & -1 & 0 \\ 0 & 0 & 0 & -1 \end{pmatrix} \tag{2.4}$$

respectively.

Next, we define the equations of motion for a test particle under the influence of gravity in a given spacetime. Since gravity is not seen as a force but a consequence of spacetime curvature the equations of motion are reminiscent of the Newtonian relation $\sum \mathbf{F} = 0$. Instead of always being straight lines however, the paths of these particles follow the timelike geodesics of the spacetime. These geodesics are defined by:

$$V^c \nabla_c V^a = 0 \tag{2.5}$$

where $V^a = \frac{\partial x^a}{\partial \tau}$ is a vector representing the 4-velocity of the particle or equivalently

the vector field tangent to the path of the particle. The symbol ∇_c is the covariant derivative and τ is an affine parameter which we associate with the proper time of the particle.

This equation is tensorial which means it holds for any spacetime in any coordinates, similar to vector equations from Newtonian mechanics which are coordinate independent. After a particular spacetime is specified and coordinates are chosen, the equation can be rewritten as a set of four second order ordinary differential equations which specify the path of the particle. This dependence on the geometry means that different spacetimes can in principle have very different orbits. For example using the Minkowski metric in cartesian like coordinates the equations of motion are

$$\frac{d^2t}{d\tau^2} = 0 \quad \frac{d^2x}{d\tau^2} = 0 \quad \frac{d^2y}{d\tau^2} = 0 \quad \frac{d^2z}{d\tau^2} = 0 \tag{2.6}$$

where τ is the proper time of the particle. Since the Minkowski spacetime physically corresponds to a universe with no matter the geodesics of the spacetime are straight lines. Since there is nothing to orbit in such a universe we will proceed to spacetimes that admit bound orbits.

2.1 Schwarzschild

The simplest solution to the Einstein equations which leads to orbital motion was found by Karl Schwarzschild in 1915. This solution assumes a spherically symmetric matter source like a star. The symmetry of the matter is assumed to extend to the entire spacetime. Since the physics of the spacetime is independent from the coordinates used, by choosing appropriate coordinates we can simplify calculations. In the Schwarzschild solution we typically use coordinates that make the metric diagonal.

In relativistic units the metric or line element is:

$$ds^2 = \left(1 - \frac{2m}{r}\right) dt^2 - \left(1 - \frac{2m}{r}\right)^{-1} dr^2 - r^2 d\theta^2 - r^2 \sin^2\theta d\phi^2 \tag{2.7}$$

where m is the geometric mass of the star and (t, r, θ, ϕ) are coordinates corresponding to time and familiar spherical polar coordinates. The geometric mass m, so called because it has units of length, is related to the physical mass M of the object by:

$$m = \frac{GM}{c^2} \tag{2.8}$$

where G is Newton's gravitational constant and c is the velocity of light in vacuum.

We first draw attention to the singular behavior of the metric at $r = 2m$. This relation defines the Schwarzschild radius, or the location of the event horizon of a black hole. Any stable particle orbit must stay outside this radius.

With the geometry of the spacetime specified by the metric and useful coordinates chosen to express the metric we find the geodesic equations for this spacetime are

$$\frac{d^2t}{d\tau^2} = -\frac{2m}{r\,(r-2m)} \frac{dt}{d\tau} \frac{dr}{d\tau} \tag{2.9}$$

$$\frac{d^2r}{d\tau^2} = \frac{m}{r\,(r-2m)} \left(\frac{dr}{d\tau}\right)^2 + (r-2m) \left[\left(\frac{d\theta}{d\tau}\right)^2 + \sin^2\theta \left(\frac{d\phi}{d\tau}\right)^2 - \frac{m}{r^3}\left(\frac{dt}{d\tau}\right)^2\right] \tag{2.10}$$

$$\frac{d^2\theta}{d\tau^2} = -\frac{2}{r} \frac{dr}{d\tau} \frac{d\theta}{d\tau} + \sin\theta\cos\theta \left(\frac{d\phi}{d\tau}\right)^2 \tag{2.11}$$

$$\frac{d^2\phi}{d\tau^2} = -\frac{2}{r} \frac{dr}{d\tau} \frac{d\phi}{d\tau} - \frac{2\cos\theta}{\sin\theta} \frac{d\theta}{d\tau} \frac{d\phi}{d\tau}\,. \tag{2.12}$$

In the test particle approximation these equations govern the motion of the particle around the star where τ is the particle's proper time. Consideration of these equations reveals them as coupled and nonlinear so we solve them numerically. By experimenting with different initial conditions we explore the different types of orbits allowed by this spacetime.

As a first check one might notice that far away from the star the particle trajectories appear very similar to those specified by Newtonian gravity. By considering orbits closer to the star the elliptical orbit of the particle would begin to precess around the star (see Fig. 2.1). This effect is seen as one of the experimental successes of general relativity. Specifically, this aspect of the theory predicts the perihelion precession of Mercury more accurately than Newtonian gravity [8].

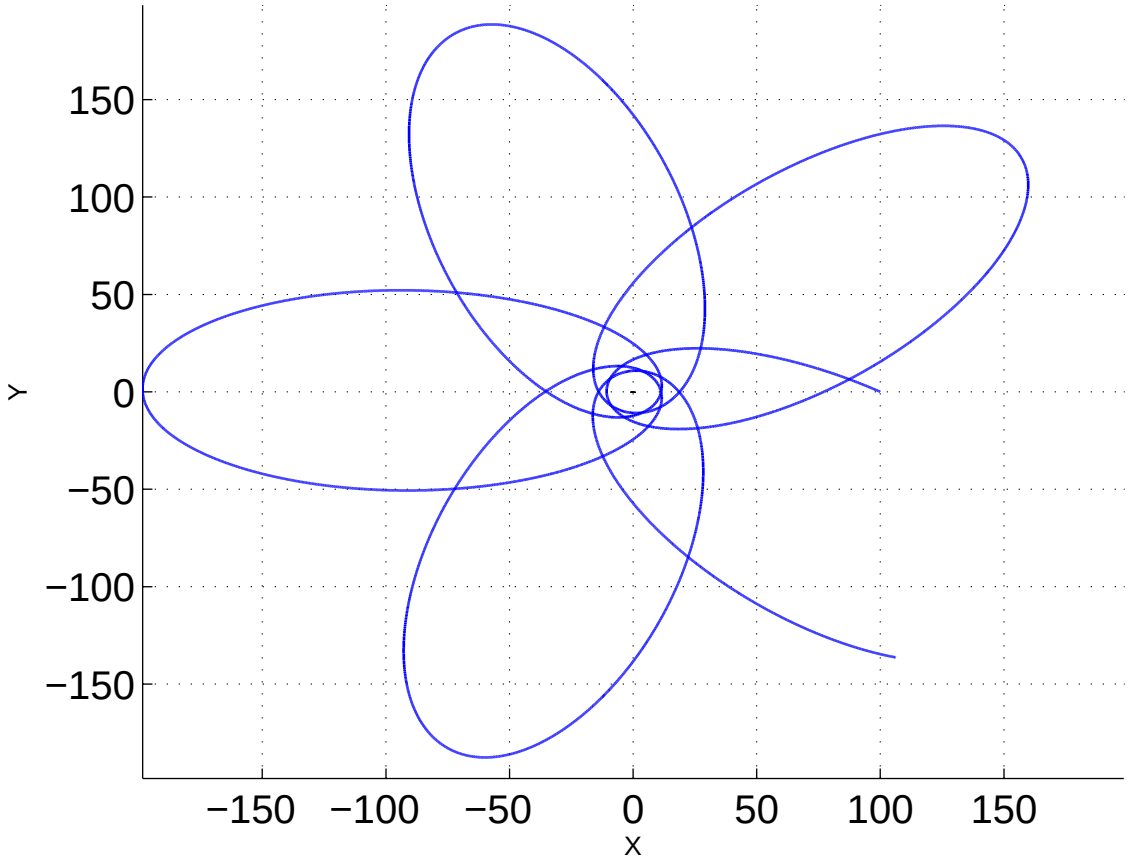

Figure 2.1 The orbital precession of a test particle with initial position at $r = 100m$ and conserved quantities $E = 0.995$ and $L = 5$. In this case, a test particle orbits a central mass, with $m = 1$, in the Schwarzschild spacetime. This is an exaggerated example of the perihelion precession of Mercury.

2.1.1 Symmetries and Conserved Quantities

Even though there is no general closed form solution to these equations, we can use them to predict some aspects of the system. First, notice that if we initially set $\theta = \frac{\pi}{2}$ and $\frac{d\theta}{d\tau} = 0$, then nothing causes θ to change during the subsequent evolution. This implies that if the particle starts in the equatorial plane of the system then it will stay in that plane. We then claim that, due to spherical symmetry, the motion of a particle with arbitrary initial conditions is constrained to move in a plane. When numerically solving the equations we usually take the equatorial case because it simplifies the equations while remaining completely general.

Another way to simplify the equations is to find and use conserved quantities. We begin this process by recalling the Killing vectors of the spacetime. A Killing vector X^a points along some symmetry of the spacetime. In other words moving in the direction of a Killing vector doesn't change the the metric. These vectors are defined as a solution to:

$$\nabla_a X_b + \nabla_b X_a = 0 \tag{2.13}$$

or equivalently

$$X^e \partial_e g_{ab} + g_{ad}\partial_b X^d + g_{db}\partial_a X^d = 0. \tag{2.14}$$

We use Killing vectors to show that there are conserved quantities throughout the particle's motion. In particular, the quantity $V^a X_a$ will be constant along any geodesic that has V^a as its tangent vector. This can be shown easily by:

$$V^b \nabla_b \left(V^a X_a\right) = V^b V^a \nabla_b X_a + X_a V^b \nabla_b V^a \tag{2.15}$$

$$= 0 \tag{2.16}$$

where we have used the antisymmetry of $\nabla_b X_a$ multiplied by the symmetric product of vectors to show the first term is zero, and (2.5) to show the second term is zero.

This demonstrates that the inner product of a Killing vector with the tangent vector of a geodesic is constant along that geodesic. Recalling that V^a is defined as the tangent to the geodesic we see that for any unique Killing vector X_a the scalar function $V^a X_a$ is constant along that path. This property allows us to define as many constants of the particle motion as there are unique Killing vectors in the spacetime.

Using the second version of Killing's equation and the fact that the metric is independent of t and ϕ we find two Killing vectors and label them ${}^{(t)}X^a = (1, 0, 0, 0)$ and ${}^{(\phi)}X^a = (0, 0, 0, 1)$. Using these vectors we find two constants of the motion which can be used to further simplify the equations of motion.

$$E = \left(1 - \frac{2m}{r}\right) \frac{dt}{d\tau} \tag{2.17}$$

$$L = r^2 \sin^2 \theta \frac{d\phi}{d\tau} \tag{2.18}$$

Note that the constants of motion are associated with the energy and angular momentum of the orbiting particle.

Inserting these quantities into the geodesic equations reduces the second order equations in t and ϕ to first order and allows us to replace the t and ϕ derivatives with simpler functions in the remaining equations.

We can also use these conserved quantities to check our numerical solutions. Without using them to simplify the equations we can check the value of E and L throughout the particle orbit. If they remain constant then we feel more confident that numerical error is small and our numerical integrators are accurate.

2.1.2 Knife Edge Orbits

As we consider orbits that become closer to the center of the spacetime we find some orbits that are radically different from our Newtonian intuition. These orbits have large scale precession. In addition, they have small tight loops around the center of

the system. Using Fig. 2.2 as an example note that the particle completes two small circular orbits at $r = 4m$ for each large ellipse that extends to $r = 200m$. Due to the inner radius of these loops they can not occur around a star, but they are possible for particles orbiting a black hole. To understand why these orbits occur we construct the so-called effective potential for this spacetime.

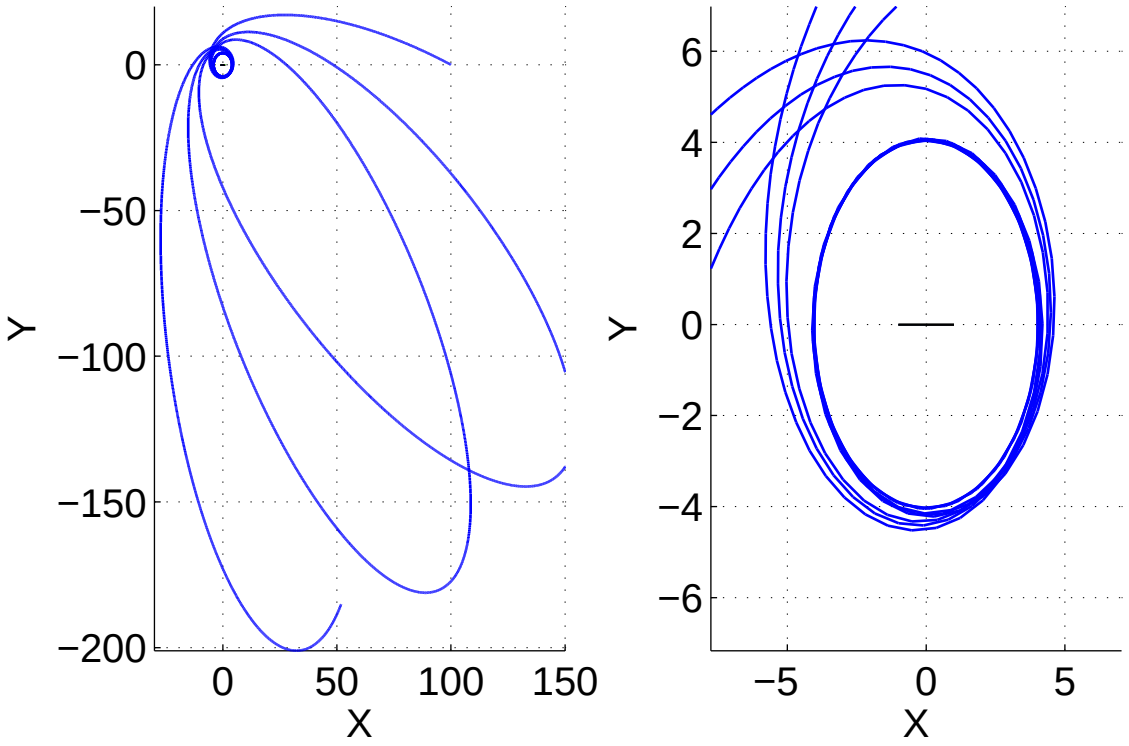

Figure 2.2 We see a knife edge orbit with two inner loops for every large elliptical orbit in the Schwarzschild spacetime with $E = 0.995$ and $L = 3.962$. On the left we see that the inner loops are small compared to the ellipses which extend out to $r = 200m$. On the right we see a close up of the small inner loops with $r = 4m$. The horizontal at the origin represents the diameter of the black hole's event horizon. Note also that this orbit corresponds to the effective potential and larger energy value in Fig. 2.3

To construct the effective potential we first take the inner product of the velocity

vector with itself.

$$\begin{aligned} V^a V_a &= g_{ab} V^a V^b = 1 \\ &= \left(1 - \frac{2m}{r}\right)\left(\frac{dt}{d\tau}\right)^2 - \left(1 - \frac{2m}{r}\right)^{-1}\left(\frac{dr}{d\tau}\right)^2 - r^2\left(\frac{d\theta}{d\tau}\right)^2 - r^2 \sin^2\theta \left(\frac{d\phi}{d\tau}\right)^2 \end{aligned} \tag{2.19}$$

Then, we substitute in the constants of the motion.

$$\left(\frac{dr}{d\tau}\right)^2 = E^2 - \left(1 - \frac{2m}{r}\right)\left(1 - \frac{L^2}{r^2}\right) \tag{2.20}$$

We then associate $\left(\frac{dr}{d\tau}\right)^2$ with a rescaled kinetic energy T and E^2 with the total energy. Assuming an equation like conservation of energy $E^2 = T + V_{\text{eff}}$ we make the identification:

$$V_{\text{eff}} = \left(1 - \frac{2m}{r}\right)\left(1 + \frac{L^2}{r^2}\right) \tag{2.21}$$

Plotting this potential against r, which is measured in terms of the geometric mass m, for different values of L we can change the shape of the potential(as in Fig. 2.3). For small enough L this potential has no maximum. In this case no stable orbits exist; any particle following an ingoing trajectory will be captured by the black hole. For large L this peak emerges in the potential close to $r = 2m$. In Fig. 2.3 we can see examples of "Knife Edge" potentials (this term was first used by Ruffini and Wheeler in *The Significance of Space Research for Fundamental Physics* in 1970). Specifically, the three potentials of largest L have a sharp peak near $r = 5m$ which is called the knife edge of the potential. The figure also shows dotted horizontal lines which correspond to particle energies. These energies lead to different orbital behavior.

As in Newtonian mechanics the particle must have an energy value larger than the potential for an orbit to exist. For example, the lower energy line in Fig. 2.3 crosses the topmost potential at $r = 3m$, $r = 8m$, and $r = 23m$. These crossing points correspond to two possible trajectories for a particle with this energy. A particle with

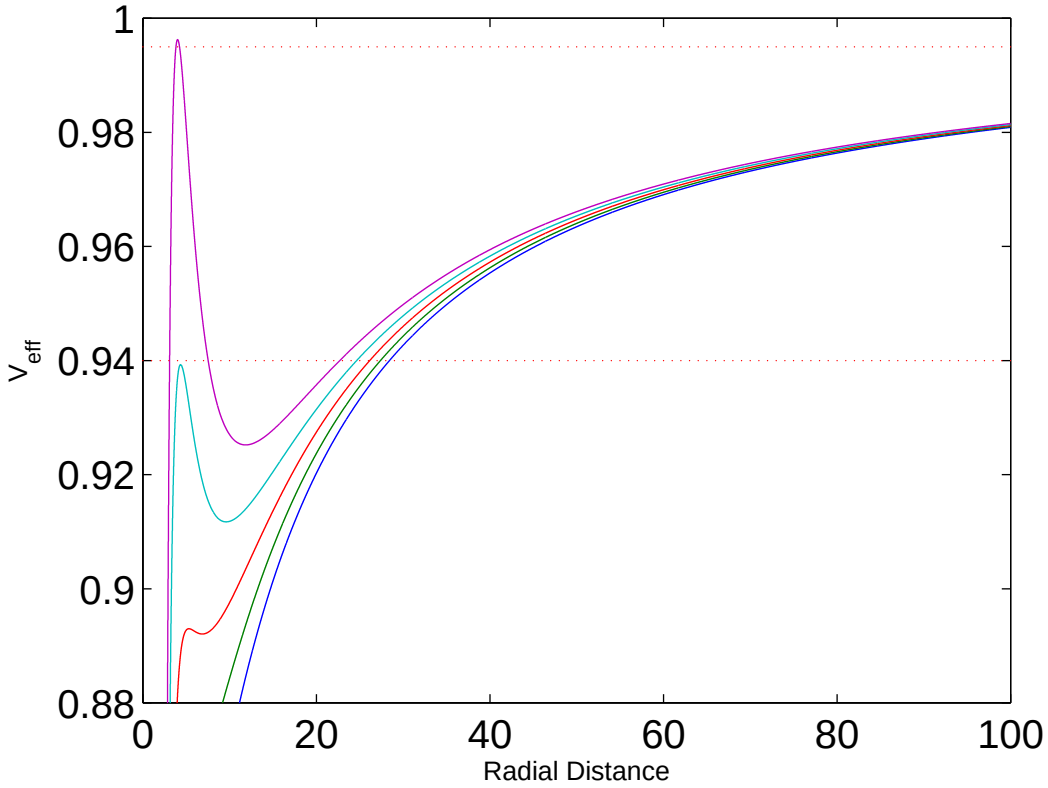

Figure 2.3 The effective potential in the Schwarzschild spacetime varying between $L = 3.00$ to $L = 3.9685$,where this last potential has the tallest peak, by equal steps. Here r measured in units of the geometric mass. The "Knife Edge" of the upper three potentials are the sharp peaks close to $r = 5m$. Lines of $E^2 = 0.995$ and $E^2 = 0.94$ are shown, the largest of which corresponds to a knife edge orbit in Fig. 2.2.

this energy which is at $r \leq 3m$ is not bound by the potential and will be captured by the black hole. The other trajectory is a bounded orbit in which the particle moves between $r = 8m$ and $r = 23m$. These r values, namely $r = 8m$ and $r = 23m$, are the turning points of the particle's orbit and are exactly analogous to the turning points of Newtonian mechanics.

The energy line with $E^2 = 0.995$ corresponds to the orbit from Fig. 2.2, so we expect turning points at $r = 5m$ and $r = 200m$ (note that the $r = 200m$ turning point is not shown in Fig. 2.3). As the particle approaches the $r = 5m$ turning

point the radial velocity goes to zero. At the same time, the conservation of L (see equation (2.18)) causes $\frac{d\phi}{d\tau}$ to increase as r decreases. This causes the orbiting particle to complete many orbits at radii close to $r = 5m$ before moving further away from the center of the spacetime.

2.2 Charged Masses and Test Particles

One extension of the Schwarzschild solution is to give the central body electric charge. This result is called the Reissner-Nordström solution. The end result is to obtain the same line element as in (2.7) with $\left(1 - \frac{2m}{r}\right)$ becoming $\left(1 - \frac{2m}{r} + \frac{Q^2}{r^2}\right)$, where Q is the electric charge of the central body measured in geometric units. This changes the location of the event horizon to $r = m + \sqrt{m^2 - Q^2}$.

When $m = Q$ the event horizon is at the smallest r value allowed by this spacetime, and this is called the extremal case. If $m < Q$ then the spacetime is said to have a naked singularity. These spacetimes are believed to be unphysical, so we use $m = Q$ as a limit on possible values of Q.

The change to $\left(1 - \frac{2m}{r} + \frac{Q^2}{r^2}\right)$ affects the effective potential and the equations of motion in the same way as the metric. Because of the similarity of the spacetime the types of test particle orbits are identical to the Schwarzschild case. The conserved quantities E and L are also similar. That is

$$E = \left(1 - \frac{2m}{r} + \frac{Q^2}{r^2}\right) \frac{dt}{d\tau} \tag{2.22}$$

and L is identical to (2.18).

The orbits in Reissner-Nordström have the same form as Schwarzschild orbits. When the charge of the central mass is increased the knife edge peak in the effective potential becomes taller, but the types of allowed orbits remain unchanged.

When we add electric charge to the test particle the behavior changes. Due to the electric force between the two charges the particle leaves the geodesics of the Reissner-Nordström spacetime. The equations of motion now take on the form:

$$V^c \nabla_c V^a = q V_b F^{ba}. \tag{2.23}$$

Where q is the charge per mass of the test particle and F^{ba} is an antisymmetric tensor called the Maxwell field tensor. This tensor keeps track of both the electric and magnetic fields in general relativity. Though F^{ba} can, in general, be complicated it is simple in the spherically symmetric case. The only non-zero components are $F_{rt} = -F_{tr} = \frac{Q}{r^2}$.

Because the Maxwell tensor is simple, only the differential equations in t and r from the non-charged case receive an extra term. Since the θ equation is unchanged from the uncharged Schwarzschild case the orbits remain restricted to the plane. Also, since the ϕ equation is unchanged we find the same conserved quantity associated with the angular Killing vector as in (2.18).

In the case of the timelike Killing vector we have to be more creative to find the corresponding conserved quantity. Consider:

$$V^c \nabla_c \left({}^{(t)}X_a V^a - \frac{qQ}{r} \right) = V^a V^c \nabla_c {}^{(t)}X_a + {}^{(t)}X_a V^c \nabla_c V^a - qQ V^c \partial_c \frac{1}{r} \tag{2.24}$$

where is ${}^{(t)}X^a = (1, 0, 0, 0)$ as before. The first term on the right hand side vanishes in the same way as in (2.15), but we then use (2.23) on the second. So,

$$V^c \nabla_c \left({}^{(t)}X_a V^a - \frac{qQ}{r} \right) = -\frac{qQ}{r^2}\frac{dr}{d\tau} - qQ \frac{dx^c}{d\tau}\frac{\partial}{\partial x^c}\frac{1}{r} \tag{2.25}$$

$$= -\frac{qQ}{r^2}\frac{dr}{d\tau} - qQ \frac{d}{d\tau}\frac{1}{r} \tag{2.26}$$

$$= -\frac{qQ}{r^2}\frac{dr}{d\tau} + \frac{qQ}{r^2}\frac{dr}{d\tau} = 0. \tag{2.27}$$

Which allows us to state that

$$E = \frac{dt}{d\tau}\left(1 - \frac{2m}{r} + \frac{Q^2}{r^2}\right) - \frac{qQ}{r} \tag{2.28}$$

is a constant of the motion.

We can also construct an effective potential for this system using these conserved quantities, but it now depends on both L and E.

$$V_{\text{eff}} = \left(1 - \frac{2m}{r} + \frac{Q^2}{r^2}\right)\left(1 + \frac{L^2}{r^2}\right) - \frac{2EqQ}{r} - \left(\frac{qQ}{r}\right)^2 \tag{2.29}$$

This complication prevents bound orbits from forming when either Q or q is much larger than the other and both have the same polarity. We can see an example of $q = \pm 0.9$ and $Q = 0.1m$ in Fig. 2.4. Notice how for fixed E and L the knife edge is suppressed to below the energy line when q and Q have the same polarity. When Q and q have similar magnitude and similar polarity, or both charges are very small, the orbits behave in the same way as previous cases. When q and Q have opposite polarity the situation reverses; bound orbits form when the magnitudes are different, and bound orbits are prevented when the magnitudes are similar.

2.3 Kerr and Kerr-Newman

The next solution to the Einstein equations models the spacetime of an axially symmetric mass spinning about an axis. This spacetime has less symmetry than previous solutions and is correspondingly more complicated. Consider the following line element of the Kerr solution:

$$ds^2 = \frac{\Delta}{\rho^2}\left(dt - a\sin^2\theta d\phi\right)^2 - \frac{\sin^2\theta}{\rho^2}\left[\left(r^2 + a^2\right)d\phi - adt\right]^2 - \frac{\rho^2}{\Delta}dr^2 - \rho^2 d\theta^2 \tag{2.30}$$

where $\Delta = r^2 - 2mr - a^2$ and $\rho^2 = r^2 + a^2\cos^2\theta$ and a is related to the angular velocity of the central mass.

Noting the cross terms in $dtd\phi$, we see that the metric is no longer diagonal. This complicates calculations and gives rise to much more interesting behavior in the geodesic equations. The knife edge orbits of previous spacetimes show up in Kerr also,

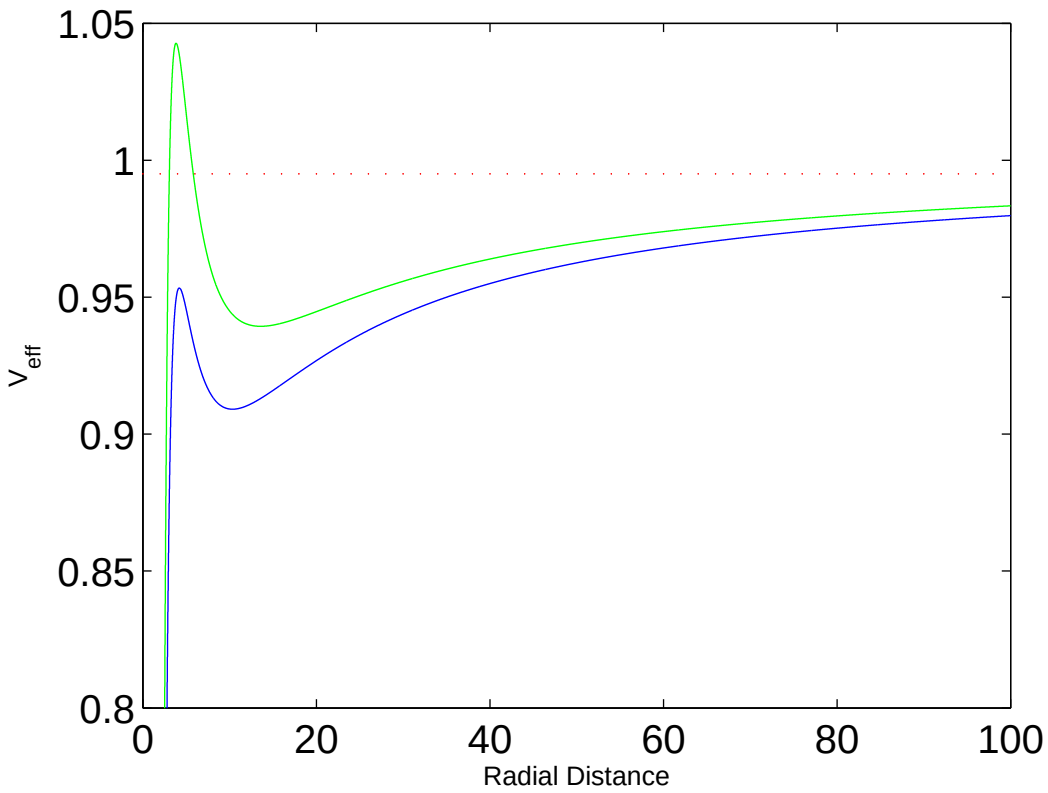

Figure 2.4 The effective potential in the Reissner-Nordström with $L = 3.9685$ and $E^2 = 0.995$. These are the identical parameters from the topmost potential from Fig. 2.3. The potential come from equation (2.29) with $q = \pm 0.9$ and $Q = 0.1m$. Notice how this prevents a stable orbit from forming (i.e. the peak of the potential is below the energy line) when q and Q have the same polarity (the lower potential).

but with more variety. The particle might move with the spin of the black hole or against it and can cross the black hole's rotational axis. See Fig. 2.5 for an example of this last type.

Since (2.30) is independent of t and ϕ there are still two Killing vectors of the spacetime. These lead to conserved quantities:

$$E = \frac{dt}{d\tau}\frac{\rho^2 - 2mr}{\rho^2} + \frac{d\phi}{d\tau}\frac{2amr\sin^2\theta}{\rho^2} \tag{2.31}$$

$$L = \frac{d\phi}{d\tau}\frac{\sin^2\left(\rho^2\left(r^2+a^2\right) + 2a^2mr\sin^2\theta\right)}{\rho^2} - \frac{dt}{d\tau}\frac{2amr\sin^2\theta}{\rho^2}. \tag{2.32}$$

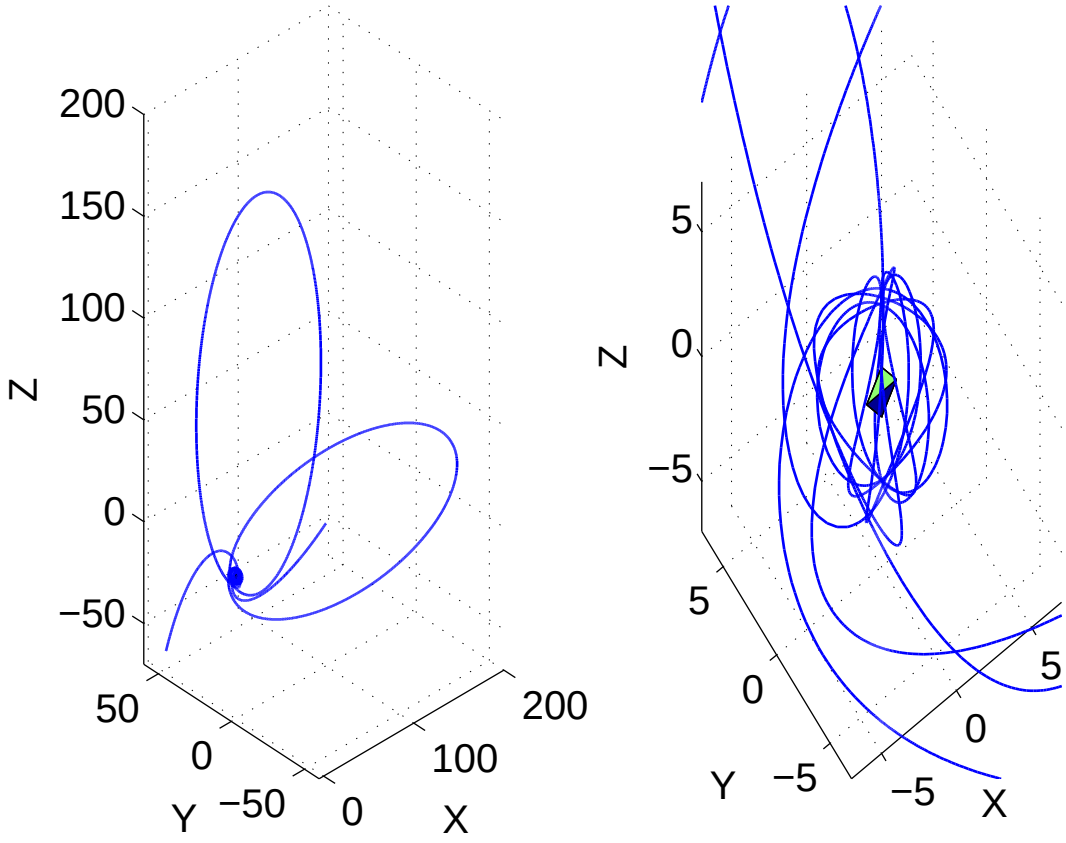

Figure 2.5 A knife edge orbit in the Kerr spacetime with $E = 0.995$ and $L = -0.00975$. Note that these orbits leave the equatorial plane, but keep about the same bounds in r as Fig. 2.2. This particular orbit leaves the plane so drastically because its path moves through the rotational axis of the black hole.

Note that in the limit of $a = 0$ we recover the conserved quantities of Schwarzschild. When $a \neq 0$ however we find a mixing of t and ϕ that is counter to our usual intuition about energy and angular momentum.

For the Kerr spacetime we find the location of the event horizon to be at $r = m + \sqrt{m^2 - a^2}$. Similar to Reissner-Nordström when $m = a$ the spacetime is said to be extremal and we use this relation as a limit on the physical values of a.

This spacetime can also be adapted to account for electric charge in the spinning

mass. In this case we retain the form of (2.30) and let $\Delta = r^2 - 2mr + a^2 + Q^2$, which puts the event horizon at $r = m + \sqrt{m^2 - Q^2 - a^2}$. This is called the Kerr-Newman solution and has orbits very similar to Kerr just as orbits in the Reissner-Nordström spacetime are very similar to Schwarzschild. When modeling a charged test particle the equations of motion become more complicated since the Maxwell tensor does not have the same simple form as the spherically symmetric case.

Notice that though these models become more and more complex and give rise to correspondingly complex behavior, there has been no mention of chaos. These models have integrable Hamiltonians and therefor cannot be chaotic as they now stand [9] [10]. In the next chapter we will introduce a model that allows chaotic orbits.

Chapter 3

Spinning Test Particle

3.1 Papapetrou Equations

General relativity is the physical model for strongly gravitating systems in astrophysics and astronomy. The spacetimes mentioned in Chapter 2 are applied to the models of what we see and expect to exist in the cosmos. With such spacetimes we can model the motion of planets and other objects orbiting stars and black holes as long as the orbiting object satisfies the test particle approximation. This requires the orbiting object to be much smaller than the central body. In this regime we can use the geodesic equations to model the orbital behavior.

Now, as we consider the orbiting bodies we are familiar with, such as the Earth, we notice that they are often spinning bodies. To model this behavior we must include more information about the moments of inertia of the object. By including higher order multipole moments of a spinning particle we can more accurately represent these physical systems. In the 1950's and 1960's work was done to model the behavior of a spinning test particle in a given spacetime with higher order multipole moments.

The equations we will use are those derived by Papapetrou [11] and reformulated

by Dixon [12]. These equations model the pole-dipole approximation. That is to say, we describe the particle as a mass monopole and spin dipole. Similar to the trajectories of a charged particle discussed in Chapter 2 a spinning particle does not follow the geodesics of the spacetime. Instead of the comparatively simple geodesic equation, the equations of motion for a spinning test particle are:

$$V^c \nabla_c P^a = -\frac{1}{2} R^a{}_{bcd} V^b S^{cd} \tag{3.1}$$

$$V^c \nabla_c S^{ab} = P^a V^b - P^b V^a \tag{3.2}$$

where V^a and P^a are the velocity and momentum of the particle respectively. The quantity $R^a{}_{bcd}$ is the Riemann curvature tensor and S^{ab} is the spin tensor of the particle.

The spin tensor keeps track of the intrinsic angular momentum associated with a spinning particle. If we recall Newtonian mechanics, angular momentum $\mathbf{L}$ is usually represented as $\mathbf{L} = \mathbf{r} \times \mathbf{p}$ where $\mathbf{r}$ is the distance from some origin about which the angular momentum is calculated and $\mathbf{p}$ is the linear momentum. Though often treated as a true vector, $\mathbf{L}$ does not transform as a regular vector under inversions, and is called a pseudo-vector. In general relativity, pseudo-vectors (such as the spin of a test particle) are expressed as antisymmetric tensors of rank two. We can then understand the Papapetrou equations as determining the motion of the particle's center of mass as well as the motion of the particle about its center of mass.

Recall that in the non-spinning case the momentum vector is just the velocity vector multiplied by the mass of the particle. In the current case, where the particle has intrinsic angular momentum, the velocity and momentum of a spinning particle do not necessarily point in the same direction. In fact, the momentum used in these equations can be defined by:

$$P^a = \mu V^a - V_b V^c \nabla_c S^{ab} \tag{3.3}$$

where μ is the mass of the particle.

An interesting feature of (3.1) is the presence of the term $R^a{}_{bcd}V^bS^{cd}$. This term shows an interaction between the curvature of the spacetime and the spin of the particle. With this term in mind we will compare the dynamics of a spinning particle traveling through regions of high or low curvature. These comparisons will help us discover how each equation affects the particle's dynamics.

Further analysis of the Papapetrou equations reveals that the system they describe is underdetermined. To fix this we must make an additional assumption or constraint. We choose the so-called supplementary condition

$$P_aS^{ab} = 0 \tag{3.4}$$

which is related to picking a center of mass frame for the particle. Some authors have made a case for using the condition $V_aS^{ab} = 0$ rather than (3.4), but we use the former condition to remain consistent with the majority of the literature, see [13] [14]. Hartl points out [3] that the difference between the two conditions is third order in the spin, so results for physically realistic spin values, which must be small, are unaffected.

These equations are clearly much more complicated than (2.5) in form. Besides this complication we have to explicitly solve for V^a in terms of P^a and S^{ab} in order to solve the equations numerically. Using the equations of motion and (3.3) Semerák [15] shows,

$$V^a = \frac{m}{-P^bP_b}\left(P^a + \frac{2S^{ab}R_{bcde}P^cS^{de}}{R_{bcde}S^{bc}S^{de} - 4P^bP_b}\right). \tag{3.5}$$

This allows us to relate the coordinates of the spacetime to the momentum of the particle.

We next consider conserved quantities. It can be shown that for a Killing vector X^a the quantity

$$C = X^aP_a + \frac{1}{2}S^{bc}\nabla_bX_c \tag{3.6}$$

is a constant of the motion. (For details see Appendix B). This means for all of the spacetimes considered in Chapter 2 we have the conserved quantities:

$$E = P_t + \frac{m}{r^2} S^{tr} \tag{3.7}$$

$$L = P_\phi - r\sin\theta \left(\sin\theta S^{\phi r} + r\cos\theta S^{\phi\theta}\right) \tag{3.8}$$

where P_t refers to the t component of the covariant momentum vector and similar for P_r etc.

There is another constant of the motion that is not the result of spacetime symmetry. The particle's total spin is conserved. The spin S of the particle is defined as the positive root of:

$$S^2 = \frac{1}{2} S_{ab} S^{ab} \ . \tag{3.9}$$

We show this quantity to be conserved by using the equations of motion and (3.4) as follows.

$$V^c \nabla_c (\frac{1}{2} S_{ab} S^{ab}) = \frac{1}{2} S^{ab} V^c \nabla_c S_{ab} + \frac{1}{2} S_{ab} V^c \nabla_c S^{ab} \tag{3.10}$$

$$= S_{ab} V^c \nabla_c S^{ab} \tag{3.11}$$

$$= S_{ab}(P^a V^b - P^b V^a) = 0 \ . \tag{3.12}$$

We should also note that the spin of the particle S is inversely proportional to $m\mu$ [3] where m is the mass of the central object and μ is the mass of the spinning particle. More explicitly, for a spinning particle of angular momentum l,

$$S = \frac{l}{m\mu} \ . \tag{3.13}$$

Since the Papapetrou equations only hold for $\mu \ll m$ (the test particle approximation) physical spin values will be very small. Consider, for example, a case of a spinning black hole acting as a test particle in orbit around a much more massive black hole.

If the orbiting black hole is extremal, or has the maximum possible intrinsic angular momentum, then $l = \mu^2$. So, the spin must satisfy,

$$S = \frac{\mu^2}{m\mu} = \frac{\mu}{m} \ll 1 \ . \tag{3.14}$$

Other astrophysical objects are believed to have intrinsic spins lower than maximal black holes. In particular Hartl puts the bounds for real astrophysical systems at about 10^{-4} to 10^{-6} in spin. [3]

3.2 Spin Vector

When solving the Papapetrou equations numerically it is advantageous to reformulate them in terms of a spin vector rather than a spin tensor. We have the freedom to do this because of the supplementary condition (3.4). It can be shown that this condition forces S^{ab} to have only 3 linearly independent components and so we can store those components in a vector rather than a tensor. For the full proof see Appendix B.

We define the spin vector by

$$S_a = \frac{1}{2}\varepsilon_{abcd}P^b S^{cd} \tag{3.15}$$

where ε_{abcd} is the totally antisymmetric Levi-Civita tensor density. We also make the following convenient definitions

$$R^*{}_{ab}{}^{cd} = \frac{1}{2}R_{abef}\varepsilon^{efcd} \tag{3.16}$$

$${}^*R^{*abcd} = \frac{1}{2}\varepsilon^{efab}R^*{}_{ef}{}^{cd}. \tag{3.17}$$

These lead to the following reformulation of the equations of motion from (3.1) and (3.2).

$$V^c\nabla_c P_a = R^*{}_{ab}{}^{cd}V^b P_c S_d \tag{3.18}$$

$$V^c\nabla_c S_a = P_a\left(R^{*b}{}_c{}^{de}S_b V^c P_d S_e\right). \tag{3.19}$$

Then (3.5) and the constants of the motion become,

$$V^a = \frac{m}{{}^*R^{*bcde}S_bP_cS_dP_e - P^bP_b}\left(P^a - {}^*R^{*abcd}S_bP_cS_d\right) \tag{3.20}$$

$$E = P_t + \frac{m}{r^4\sin\theta}\left(P_\theta S_\phi - P_\phi S_\theta\right) \tag{3.21}$$

$$L = P_\phi + \frac{1}{r}\left[P_t\left(r\cos\theta S_r - \sin\theta S_\theta\right) + S_t\left(\sin\theta P_\theta - r\cos\theta P_r\right)\right] \tag{3.22}$$

$$S^2 = S^aS_a. \tag{3.23}$$

This change is useful because where once there were six equations to solve for the spin tensor, there are now only four to solve for the spin vector. It is also numerically simpler to solve vector equations as opposed to tensor equations.

Using the Papapetrou equations we can numerically model the dynamics of a spinning particle in any given spacetime. However, in the remainder of this thesis we will restrict our attention to the Schwarzschild spacetime. Though this may at first seem a narrow view of possible orbital dynamics, the behavior we encounter is not trivial.

Chapter 4

Chaos

As mentioned in the introduction, the spinning test particle system can be chaotic. Since chaos theory is a very broad discipline we give some context to the spinning particle system in this chapter.

4.1 Overview

The field of nonlinear dynamics or chaos theory has many applications throughout the sciences. We frequently encounter physical systems in which the dynamical behavior appears to be almost random, or at least to be extremely sensitive to the initial conditions. In these systems a small change in the initial state of the system leads to a large change in the evolution of the system. Chaos theory is the study of these problems. The field of chaos has led to a better understanding and ability to predict these systems in nature, and to distinguish chaotic behavior from random behavior.

One way in which this sensitivity to initial conditions can be characterized is with with the so-called Lyapunov exponent. If we define the distance D between two phase

space trajectories as

$$D(t) = d_0 e^{\lambda t} \tag{4.1}$$

where d_0 is the initial difference between the two trajectories, then λ is defined as the Lyapunov exponent. If λ is greater than zero, then phase space trajectories diverge at an exponential rate. Thus, trajectories with $\lambda > 0$ are very sensitive to small changes in their initial conditions and are said to be chaotic. The Lyapunov exponent can also be used to measure how chaotic one trajectory is compared with another.

In addition to the quantitative Lyapunov exponent, the structure of the phase space can indicate qualitatively whether or not a system is chaotic. The canonical example is Lorenz's model of atmospheric convection currents. This model of three coupled nonlinear differential equations gives rise to what is called a strange attractor as shown in Fig. 4.1. These attractors show up in the phase space of all dissipative chaotic systems and have many interesting features including fractional dimension. In non-dissipative or Hamiltonian systems, such as the problems addressed in this thesis, these attractors do not form, and we will treat this case in more detail. We will show how Poincaré sections of the phase space can indicate whether or not a Hamiltonian system is chaotic or not.

Another qualitative way to look for chaos is to consider the power spectrum of the variables in the system. If the system is periodic, then sharp, discontinuous spikes will denote the resonant frequencies of the system. In the chaotic case the spectrum will appear continuous. The spectrum will have no clear resonant frequencies. The draw back to this method is that it can be very difficult to distinguish complex quasi-periodic behavior from true chaotic behavior.

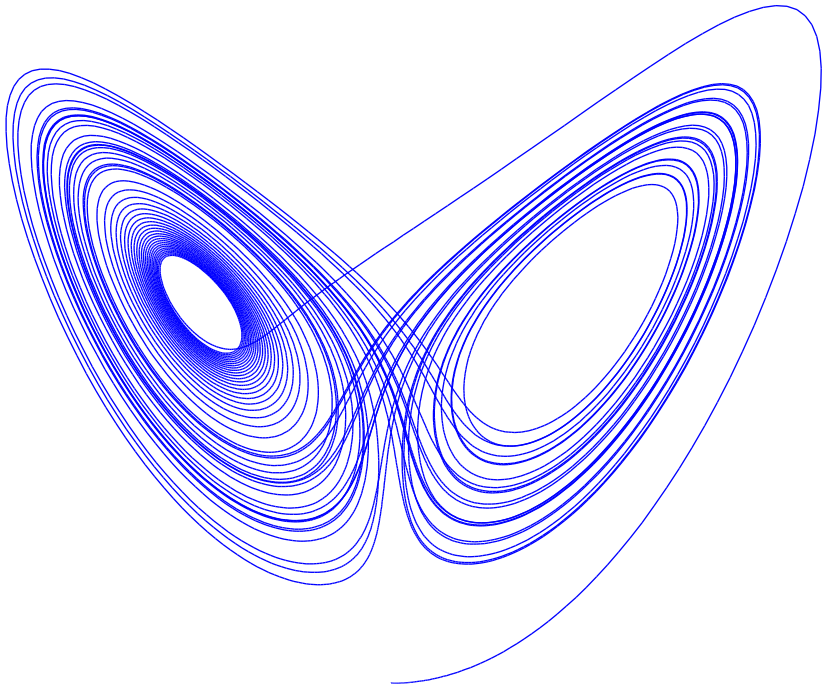

Figure 4.1 The strange attractor of Lorenz's convection model. These types of attractors appear in the phase space of many systems in fluid dynamics. They can not form in the phase space of conservative systems.

4.2 Conservative Chaotic Systems

Physical systems in which friction or dissipation of any kind is ignored are called conservative or Hamiltonian systems. As a consequence of Liouville's theorem any volume in the phase space of a conservative system must be conserved as the system evolves. This means that the phase space of conservative systems have no attractors. There is, however, structure to the phase space that is useful for understanding these systems.

In a Hamiltonian system with N degrees of freedom there will be N pairs of variables. Each pair denotes the position and conjugate momentum, typically denoted

as q_i and p_i respectively, of each degree of freedom. This leads to a $2N$ dimensional phase space for the system, which can make visualization of phase space trajectories difficult. What improves matters are conserved quantities. Every conserved quantity of the system's evolution restricts the phase space trajectories. It can be shown (see Hilborn [9] and Ott [10]) that for a system with N degrees of freedom and M conserved quantities, any phase space trajectory is confined to an $N-M$ dimensional torus embedded in the $2N$ dimensional phase space.

If we consider a plane in the phase space that intersects this torus we see that the trajectory intersects the section in a well defined torus of a lower dimension. For example, a two torus intersected by a plane traces out an ellipse on the plane as shown in Fig. 4.2

A chaotic Hamiltonian system does not have enough conserved quantities to confine the phase space trajectory to the surface of the torus. If we think of the Hamiltonian H of the system as $H = H_0 + \varepsilon H_1$ where H_0 is an integrable Hamiltonian and εH_1 as a non-integrable perturbation, then the phase space trajectories will remain close to the surface of the torus, but not exactly on the surface. The nonintegrable perturbation adds a degree of freedom that allows trajectories to wander away from the surface of the torus. In the example mentioned above the elliptical shape would still be present, but the edges would be broken up similar to Fig. 4.3. These are called KAM tori [9, 10]. Looking for KAM tori is one way to qualitatively check for chaos in a conservative system that is close to integrability.

Systems that can be described by a Hamiltonian have other properties that may preclude the possibility of chaos. A Hamiltonian which has as many constraints on the system as degrees of freedom is integrable. A system with an integrable Hamiltonian cannot be chaotic. All of the nonspinning test particle orbits considered in Chapter 2 are integrable systems and cannot be chaotic.

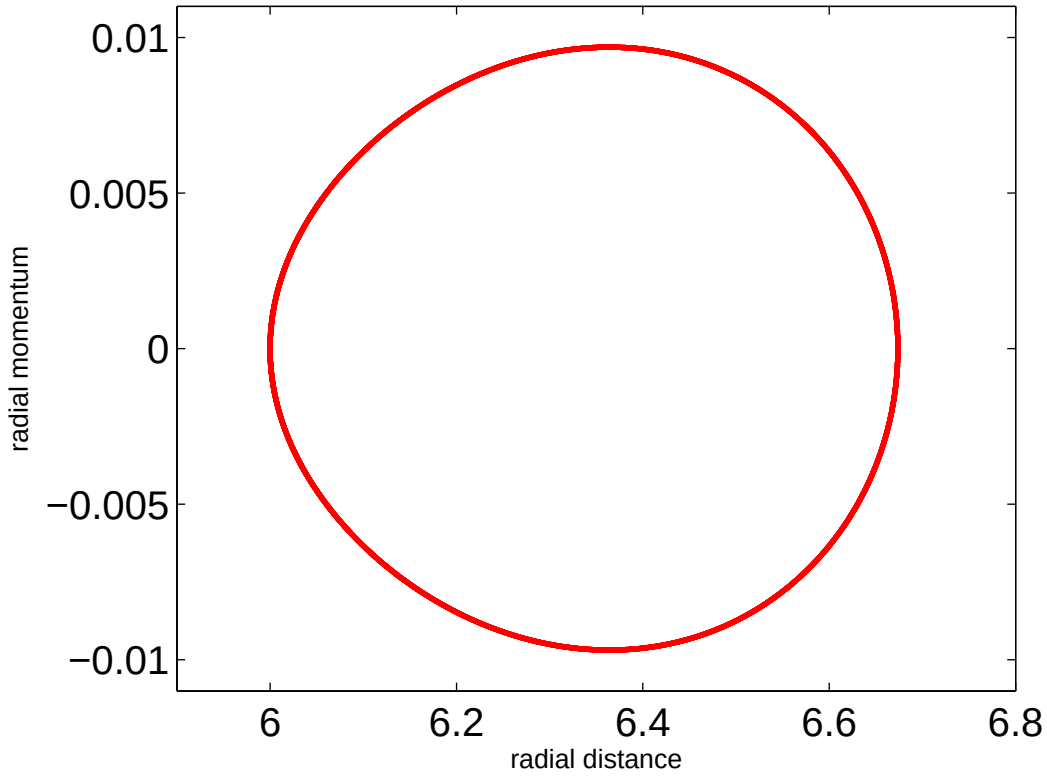

Figure 4.2 A Poincaré section of the phase space trajectory of a non-chaotic particle orbit. Notice that the trajectory is confined to the surface of a torus which intersects the section.

4.3 The Spinning Particle

In the case of the spinning test particle the spin of the particle acts as a perturbation on the Hamiltonian. This perturbation removes the integrability of the non-spinning case, making chaos possible. Note that the condition of a non-integrable Hamiltonian is necessary but not sufficient for the system to exhibit chaos. This means that every orbit, or set of initial conditions, must be checked for chaos. Still, we often find that regions of the initial condition space will be uniformly chaotic or not chaotic. With this in mind we check representative orbits from different regions to determine what conditions lead to chaos.

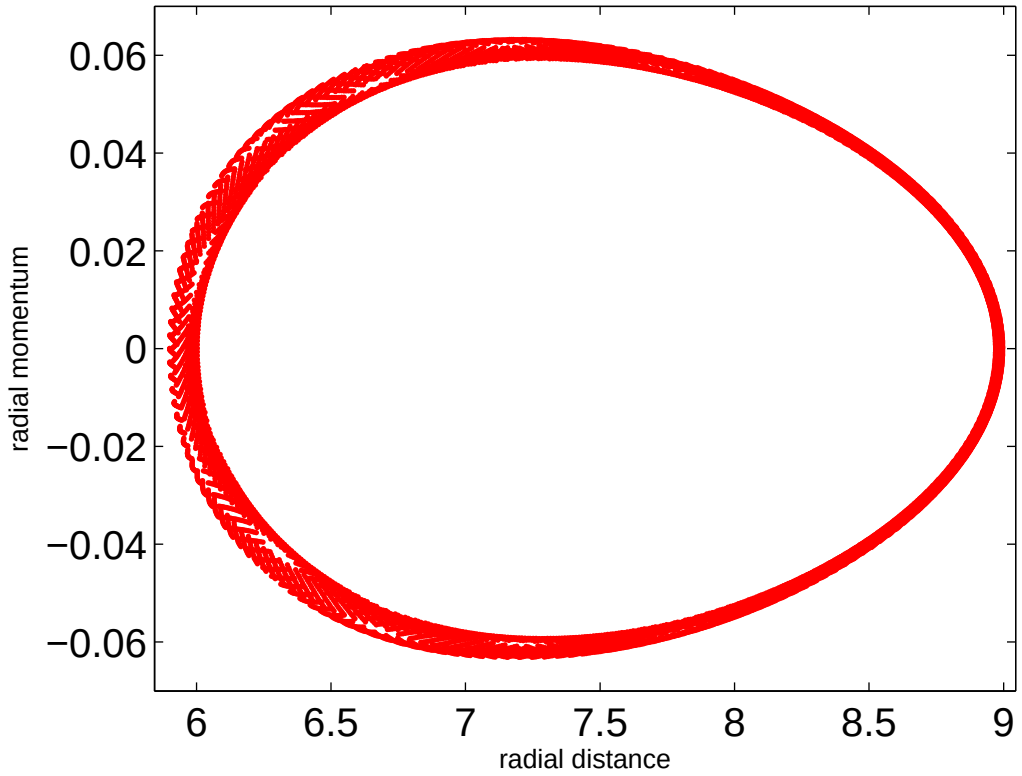

Figure 4.3 A Poincaré section of the phase space trajectory of a chaotic particle orbit. Notice that the trajectory stays close to the surface of a torus similar to Fig 4.2, but doesn't have the thin defined surface.

The increased complexity of spinning particle orbits can be seen even before considering the phase space. Recall from chapter 2 that orbits in the Schwarzschild spacetime remained in a plane, which for convenience we took to be the equatorial plane. In general spinning particles do not remain in any such plane. While the spacetime remains spherically symmetric, the particle has a defined direction of spin. In most cases the interaction between the spin and orbital angular momentum of the particle push it out of planer motion. While some initial orientations of the spin vector keep the orbit in the plane (when the spin is parallel or antiparallel to the angular momentum), in most orbits the particle has more freedom.

Since the equations of motion for the spinning particle (3.1) couple the spin tensor

to the Riemann curvature tensor, we might guess that there may be more spin effects in regions of higher curvature. In addition, the spin of the particle acts as a perturbation on the Hamiltonian, so particles that follow orbits into regions of high curvature may show more chaos than orbits that stay in regions of less curvature. Since we are interested in chaotic orbits at physically reasonable spin values, high curvature orbits will be looked at in detail.

4.3.1 Previous Results

Suzuki and Maeda [2] focus on chaotic orbits which remain close to the center of the system for the entire orbit. These orbits only travel through high curvature areas of the spacetime. They argue that only one region of the $S-L$ plane, where S and L are the spin and orbital angular momentum of the particle respectively, allows chaotic orbits. (They call this region B2 and it is shown explicitly in Fig. 3 of [2].) The heart of their argument is that the effective potential in this region is sufficiently different from the nonspinning case to allow chaotic behavior. From the boundary of this region they give a lower bound on spin required for chaos when $L = 4$ is $S = 0.635$. For lower L values the lower bound increases. For instance when $L = 3.7$ the required spin is $S = 1$. They also claim that in the Kerr spacetime the region that allows chaotic orbits includes smaller spin values as the angular momentum of the black hole increases.

Hartl [3] focuses on the Kerr spacetime rather than Schwarzschild, but does check the Schwarzschild case. He confirms the work of Suzuki and Maeda and goes on to say that the Kerr spacetime allows many more chaotic orbits than Schwarzschild. In [4] he finds no evidence for chaotic orbits with spin lower than $S = 0.1$.

Chapter 5

Looking for Chaos

Before we look for chaos in different orbits we must learn how to recognize a chaotic system. The particular system we consider is that of a spinning test particle in orbit about a spherically symmetric central mass. We use the Schwarzschild spacetime as our background and the Papapetrou equations as our equations of motion.

5.1 KAM Tori

Suzuki and Hartl claim that chaotic orbits are possible in the Schwarzschild spacetime. At the same time they report that many orbits are not chaotic. While ultimately we want a quantitative measure of chaos, namely the Lyapunov exponent, initially we must find chaotic orbits by other means. We use more qualitative methods to find a strongly chaotic orbit to test our Lyapunov exponent calculations and compare them to Suzuki and Hartl. Once we have used these methods to confirm the results in the literature we can begin extending those results.

The first method we implement is to take Poincaré sections of the phase space and look for KAM tori. Following Suzuki we choose the section defined by the $r - P_r$

plane in the phase space, where r is the coordinate distance the test particle is from the center of the central mass and P_r is the conjugate momentum. In the case where the particle has no spin a typical section looks like an oval, see Fig. 4.2.

When considering sections for spinning test particle orbits we look for this clean oval to break up as in Fig. 4.3. Looking at the section for different orbital types, we notice that when the particle is close to the center of the spacetime, $r = 0$, the torus seems to break up more. In the case of knife edge orbits with large maximal distance, such as Fig. (2.2), all of the torus looks unbroken except for the edge close to $r = 4m$.

The orbits that produce sections like Fig. 4.3 are close to the center of the spacetime and are in good agreement with the sections produced by Suzuki. These high curvature orbits seem to lead to chaotic behavior and appear to be the most likely candidates for physical chaos in the Schwarzschild spacetime.

5.2 Power Spectrum

Aperiodicity is one of the hallmarks of chaotic systems. Thus by finding the frequency spectrum of the coordinates in a system we should be able to check for periodicity or chaos. The simplest way to accomplish this is to find the power spectrum of each coordinate.

To construct a power spectrum for a coordinate $t(\tau)$ we first need the Fourier transformed coordinate $\hat{t}(\omega)$ defined by

$$\hat{t}(\omega) = \frac{1}{\sqrt{2\pi}} \int_{-\infty}^{+\infty} t(\tau) e^{-2\pi i \tau \omega} d\tau \ . \tag{5.1}$$

Then the power spectrum $P(\omega)$ of the coordinate t is defined by

$$P(\omega) = \frac{\hat{t}(\omega)\hat{t}^*(\omega)}{2\pi} \tag{5.2}$$

where * denotes complex conjugation.

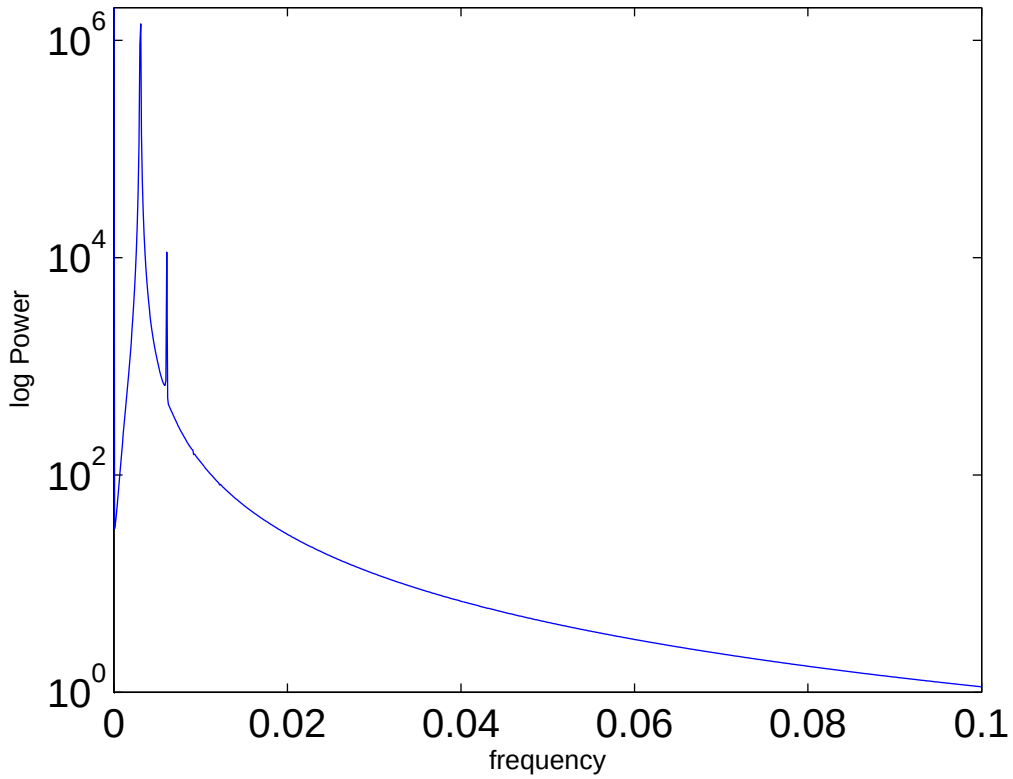

Figure 5.1 The power spectrum of the coordinate r for an orbiting particle with no spin. Since the orbit is very periodic we see one main spike denoting the frequency related to its period and a secondary spike denoting the period of precession.

Any periodic nature in this coordinate shows up in the power spectrum as a spike at the frequency of the periodicity. A simple orbiting particle in the Schwarzschild spacetime, as in Fig.5.1, has very well defined spikes showing the periodic nature of the r coordinate. Even though this orbit takes place in a region of high curvature, the spinless particle orbit remains periodic. The power spectrum shows one main spike, which corresponds to the period of its orbit, and another spike related to the period of the orbit's precession. The power spectrum for the θ coordinate for this system has no spikes since there is no motion in θ.

In contrast, the power spectrum in θ for orbits with high curvature and high spin become much more complicated (see Fig. 5.2). While the r coordinate also increases in complexity it's difficult to decidedly classify its power spectrum as chaotic or not. The change in θ is much more stark, moving from nothing at all to the complexity seen in the figure.

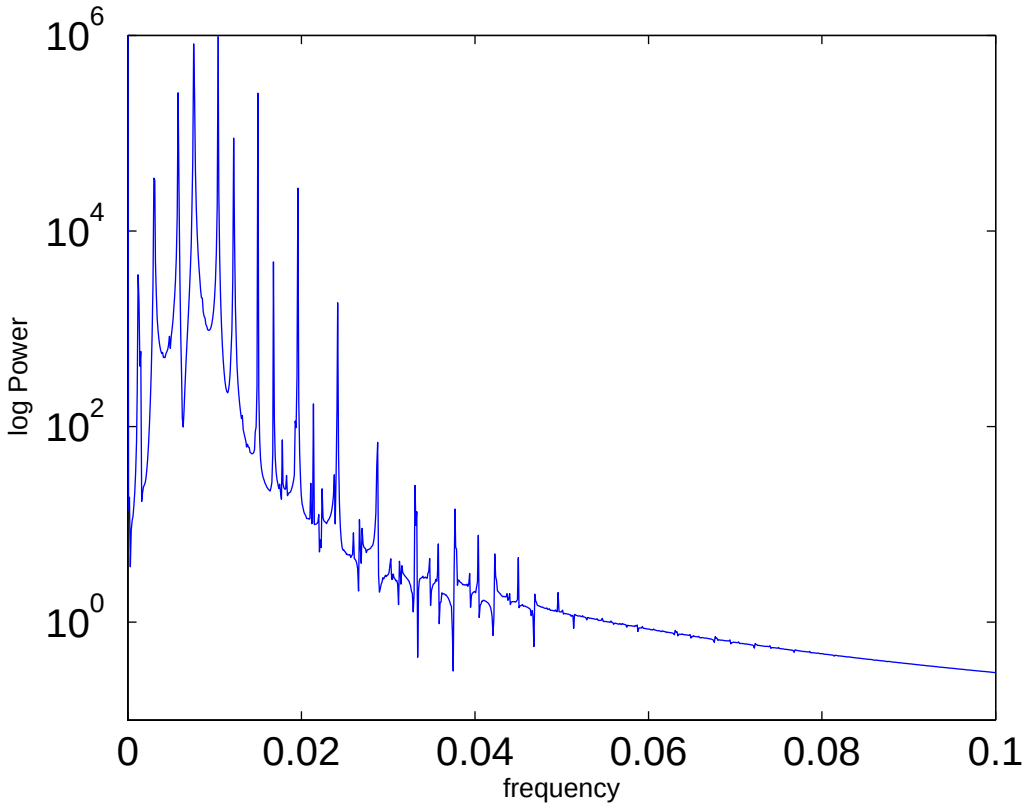

Figure 5.2 The power spectrum of the coordinate θ for an orbiting particle near the center of the Schwarzschild spacetime. Notice the increase in complexity from the nonchaotic power spectrum in Fig. 5.1.

There is no well defined way to determine if power spectra are complex enough to be chaotic. The usual qualification is that the peaks of the power spectrum become continuous. For this reason we use them only as a check on the KAM tori.

5.3 Lyapunov Exponent

A much clearer measure of chaos is the Lyapunov exponent. This measure is useful for both qualitative and quantitative measurements. The qualitative aspect comes in the sign of the exponent. If the exponent is negative or zero, then the system is not chaotic for the specific initial conditions investigated. If the exponent is positive then the system is chaotic.

This more quantitative aspect helps us compare just how chaotic orbits are in relation to each other. The larger the exponent the more chaotic the orbit. This allows us not only to define which orbits are chaotic, but also to group different orbits together by the magnitude of their Lyapunov exponent.

These exponents, defined earlier by (4.1), can be difficult to compute in general relativity. Perhaps the first method to come to mind is to evolve two nearly identical systems that differ by a very small amount in the phase space. We can then track the distance between the two phase space trajectories as a function of τ.

As τ represents the proper time of an orbiting particle, when we want to compare two particles following different orbits we must realize that each has a proper time different from the other. While the particles are close we might approximate them as having the same proper time, but as they move apart in phase space this becomes an increasingly poor assumption.

The Jacobian method used by Hartl has the advantage of sidestepping this problem. The basic idea is that we can track the growth of a vector in the tangent space of a phase space trajectory to compute the Lyapunov exponent for that trajectory (for more detail see [3] and [4]). The equation that dictates the evolution of this vector is

$$\frac{d\boldsymbol{\xi}}{d\tau} = \mathbf{Df} \cdot \boldsymbol{\xi} \tag{5.3}$$

where $\boldsymbol{\xi}$ is a vector in the tangent space, and $\mathbf{Df}$ is the Jacobian matrix of the system.

To understand this method, consider a high dimensional ellipsoid in the phase space defined by a set of initial conditions. This ellipsoid may be warped by the evolution of the system, but a consequence of Liouville's theorem is that phase space volumes are conserved. This means that the volume enclosed by this warped ellipsoid will remain constant over the course of the evolution. The axis of the ellipsoid that corresponds to a chaotic coordinate will stretch, requiring other axes to contract. The system then can have more than one chaotic coordinate, but for each chaotic coordinate there must be a nonchaotic coordinate whose values are converging at the same rate as the chaotic coordinate's values are diverging. In other words for every Lyapunov exponent that corresponds to a chaotic axis there is an exponent with the same magnitude but opposite sign.

The Jacobian method finds the largest Lyapunov exponent by evolving an arbitrary initial condition vector in the tangent space of the phase space. As the system evolves this vector lines up with the direction of greatest stretching. By considering the magnitude of this vector as a function of the proper time τ, we can then define the largest Lyapunov exponent of the system by

$$\lambda = \lim_{\tau \to \infty} \frac{\ln(\frac{|\boldsymbol{\xi}|}{|\boldsymbol{\xi_0}|})}{\tau} \tag{5.4}$$

where $\boldsymbol{\xi_0}$ denotes the initial tangent vector. Since numerically we cannot let τ go to infinity, when we calculate we will refer to the Lyapunov exponent as a function of τ,

$$\lambda(\tau) = \frac{\ln(|\boldsymbol{\xi}|)}{\tau} \tag{5.5}$$

where we have taken $|\boldsymbol{\xi_0}| = 1$.

For this last analysis we have denoted the magnitude of a vector $\boldsymbol{\xi}$ by $|\boldsymbol{\xi}|$. Recall that this vector lives in the tangent space to the phase space of our physical system. This leads to confusion about what norm to use when calculating a vector magnitude.

Eckmann [16] shows that when calculating Lyapunov exponents different norms may lead to different values, but the character of the exponent, that is whether it is positive, negative, or zero, will not be affected. With this in mind, we use the Euclidean norm for simplicity when calculating vector magnitudes.

This method can be extended to find the Lyapunov exponent corresponding to each axis of the stretching ellipsoid. Hartl implements this extended method [3] in some cases and shows that the Lyapunov exponents do come in opposite sign pairs for the spinning particle system. His results also indicate that the direction of greatest stretching is not along the axis of any coordinate or conjugate momentum. So, when we find the largest exponent we do not expect it to correspond to a particular coordinate or momentum.

5.3.1 Numerical Implementation

Two obstacles to implementing the Jacobian method are creating the Jacobian matrix of the system and extrapolating the Lyapunov exponent at $\tau = \infty$ from (5.5). This first problem is a matter of analytic calculation which can be answered exactly. The second problem deals with numeric prediction and will require careful consideration.

The Jacobian matrix of the system of a spinning test particle is 12×12 with each component a different function of the variables. Explicitly,

$$\mathbf{Df} = \begin{pmatrix} \frac{\partial \dot{x}^a}{\partial x^b} & \frac{\partial \dot{x}^a}{\partial P_b} & \frac{\partial \dot{x}^a}{\partial S_b} \\ \frac{\partial \dot{P}_a}{\partial x^b} & \frac{\partial \dot{P}_a}{\partial P_b} & \frac{\partial \dot{P}_a}{\partial S_b} \\ \frac{\partial \dot{S}_a}{\partial x^b} & \frac{\partial \dot{S}_a}{\partial P_b} & \frac{\partial \dot{S}_a}{\partial S_b} \end{pmatrix} \tag{5.6}$$

where $\dot{x}^a = V^c \nabla_c x^a$. The nine 4×4 blocks that make up this matrix can be found in coordinate independent form, and are given in the appendix of [3]. Given any metric these equations define each element of the Jacobian as a (often complicated) function

of the coordinates, the elements of the covariant momentum vector, and the elements of the covariant spin vector.

The more subtle problem is how to distinguish a small Lyapunov exponent from a zero Lyapunov exponent. In the work done by Suzuki [2] and Hartl [3, 4] the system was allowed to evolve for a specific time at which point the value of (5.5) was used as an approximation of the Lyapunov exponent. We have developed a different method which both reduces computation time and predicts the Lyapunov exponent at $\tau = \infty$.

Consider the plots of (5.5) as shown in Fig. 5.3 and Fig. 5.4. These are typical examples of how $\lambda(\tau)$ converges. Notice that the functions are modeled well by the fit

$$f(\tau) = a_1 + \frac{a_2}{\tau^{a_3}} \tag{5.7}$$

where a_1, a_2, and a_3 are constants that are varied until the root mean square error between the fit and (5.5) is minimized. More explicitly the constants are varied to minimize the function

$$err = \left(a_1 + \frac{a_2}{\tau^{a_3}} - \lambda(\tau)\right)^2. \tag{5.8}$$

This model predicts what the Lyapunov exponent for the system will be, namely a_1. For instance in Fig. 5.3 $a_1 = -3 \times 10^{-6}$ and in Fig. 5.4 $a_1 = 4.5 \times 10^{-4}$. Since the spinning particle system is conservative we cannot have negative Lyapunov exponents, because these indicate the presence of an attractor in the phase space. But in the orbit corresponding to Fig. 5.3 the root mean square error of the fit is 3×10^{-6} so the exponent value of zero is contained in the error bars of the fit. For the orbit corresponding to Fig. 5.4, the RMS error is 1.5×10^{-5} keeping zero well outside the error bars of the fit.

This model of the Lyapunov function also gives a measure of how quickly the exponent converges, $\frac{a_2}{\tau^{a_3}}$. While experimenting with this model we noticed that orbits with high spin converge faster than those with low spin. While there is a direct

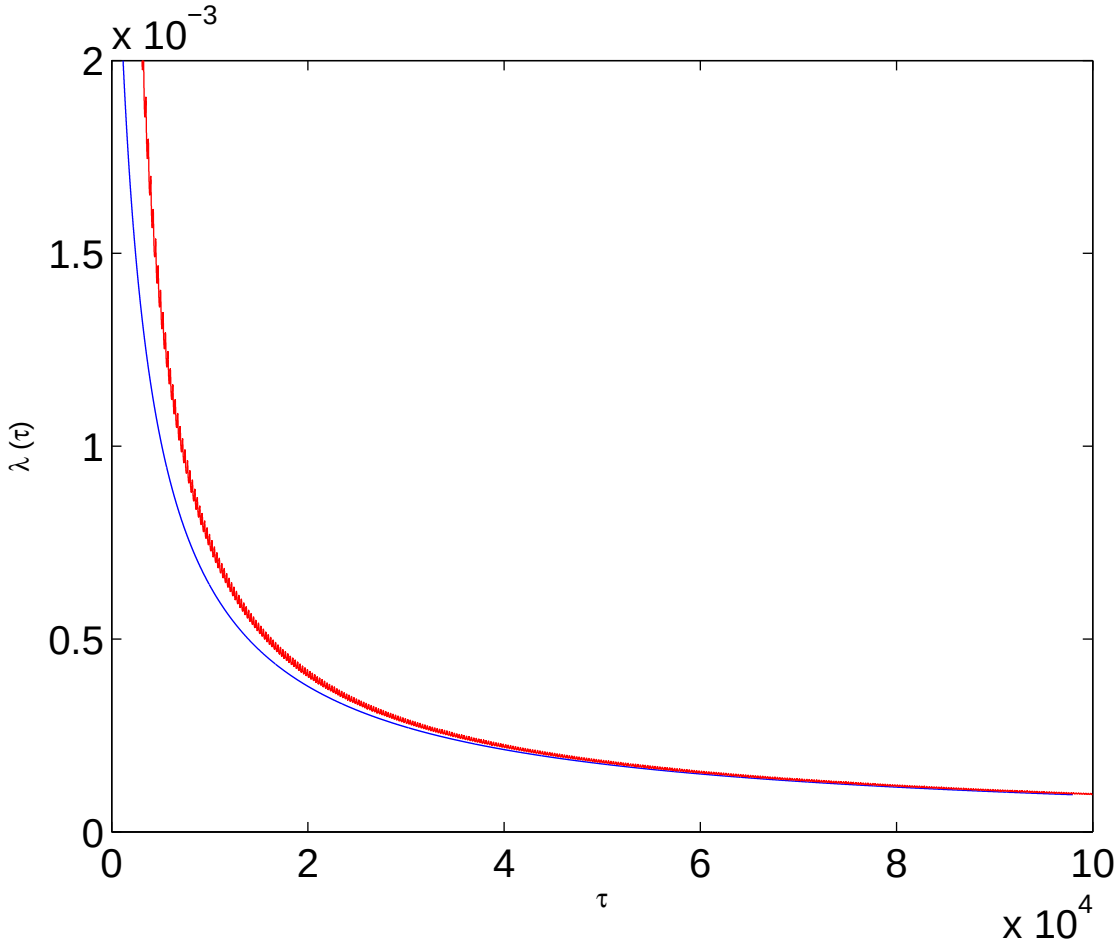

Figure 5.3 We see the jagged Lyapunov function converging to 0 for an orbit with $S = 0$. We also plot the the curve fit to the data. The predicted Lyapunov exponent for this orbit is -3×10^{-6}, but 0 is contained by the RMS error, 3×10^{-6}, of the fit.

correlation between spin and the rate of convergence there is a steep increase close to $S = 0.5$.(See Fig. 6.1)

In previous work, Lyapunov exponents with slower convergence rates have been discounted as numerical error. The difference in convergence rate between the zero point and these small spin exponents is much smaller than the difference between the zero point and the high spin exponents. Since these differing rates of convergence were not taken into account, terminating each orbit after some predetermined time

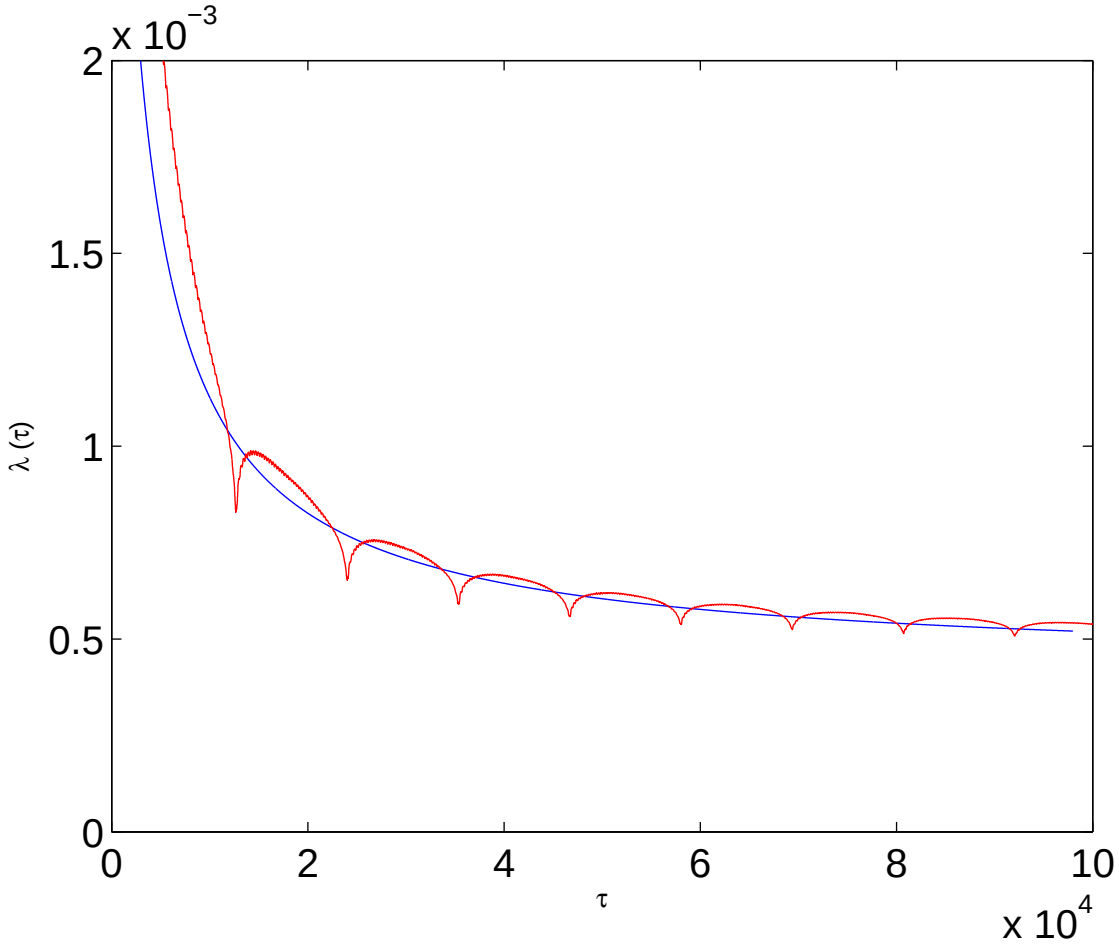

Figure 5.4 We see the jagged Lyapunov function converging to 0 for an orbit with $S = 0.3447$. We also plot the the curve fit to the data. The predicted Lyapunov exponent is 4.5×10^{-4} with 0 well out side the RMS error, 1.5×10^{-5}, of the fit.

seemed natural. Unfortunately, this inflates the zero spin exponent, which has the slowest convergence, making it difficult to distinguish from small exponent values.

Recall from chapter 4 that integrable systems cannot be chaotic and so must have a Lyapunov exponent of zero. With this in mind Suzuki and Hartl use the zero spin orbit as the zero baseline for other exponent values. When this baseline is pushed up to the range of small but nonzero exponent values, these values were discounted as numerical error.

We avoid this problem by comparing Lyapunov exponents at a uniform degree of convergence rather than a uniform time. While evolving the system we fit the function which converges to the Lyapunov exponent with (5.7) and wait until the derivative of the last few points reaches a given value close to zero. When the derivative of the fit has become sufficiently small, specifically when the value is on the order of 7×10^{-9}, we say that the function has converged. In this way we compare exponents which have all converged the same amount rather than comparing by time of evolution. We find that this method reveals more of the chaotic nature of these orbits.

In addition we can use the fit curve to predict the true Lyapunov exponent for a given orbit without integrating for infinite time. These prediction values, with their error bars, give us confidence that the true exponent is within some range of values and more importantly give a clear differentiation between positive and zero values.

Chapter 6

Results

Our primary interest in this thesis is to determine whether or not physical spin values can give rise to chaotic orbits. In this chapter we will first consider orbits similar to those considered by Suzuki and Maeda and then look at other types of orbits. Since the orbits considered by Suzuki and Maeda remain in high curvature regions for the entire orbit, the other orbital types we consider are those that remain in regions of low curvature and orbits that move through high and low curvature regions. For each orbital type we begin with a set of initial conditions with $S = 0$ and calculate the Lyapunov exponent. We then increase the magnitude of the spin and plot the Lyapunov exponents for each spin value.

6.1 High Curvature Orbits

We first consider orbits similar to those used by Suzuki and Maeda [2]. These orbits remain close to the center of the spacetime, in our first cases between $r = 6m$ and $r = 8m$, throughout the system's evolution. This confines the orbits to high curvature regions of the spacetime. This high curvature means that equation (3.1) has a

correspondingly large effect on the particle's motion.

One difference between the orbits we consider and those used by Suzuki and Maeda is the total angular momentum of the orbiting particle. They claim (by way of Fig. 3 of [2]) that stable chaotic orbits cannot occur for angular momentum $L \leq 3.6$. We begin our analysis with orbits having angular momentum of $L = 3.6$, energy $E = 0.9522$, and an initial radius of $r = 6m$.

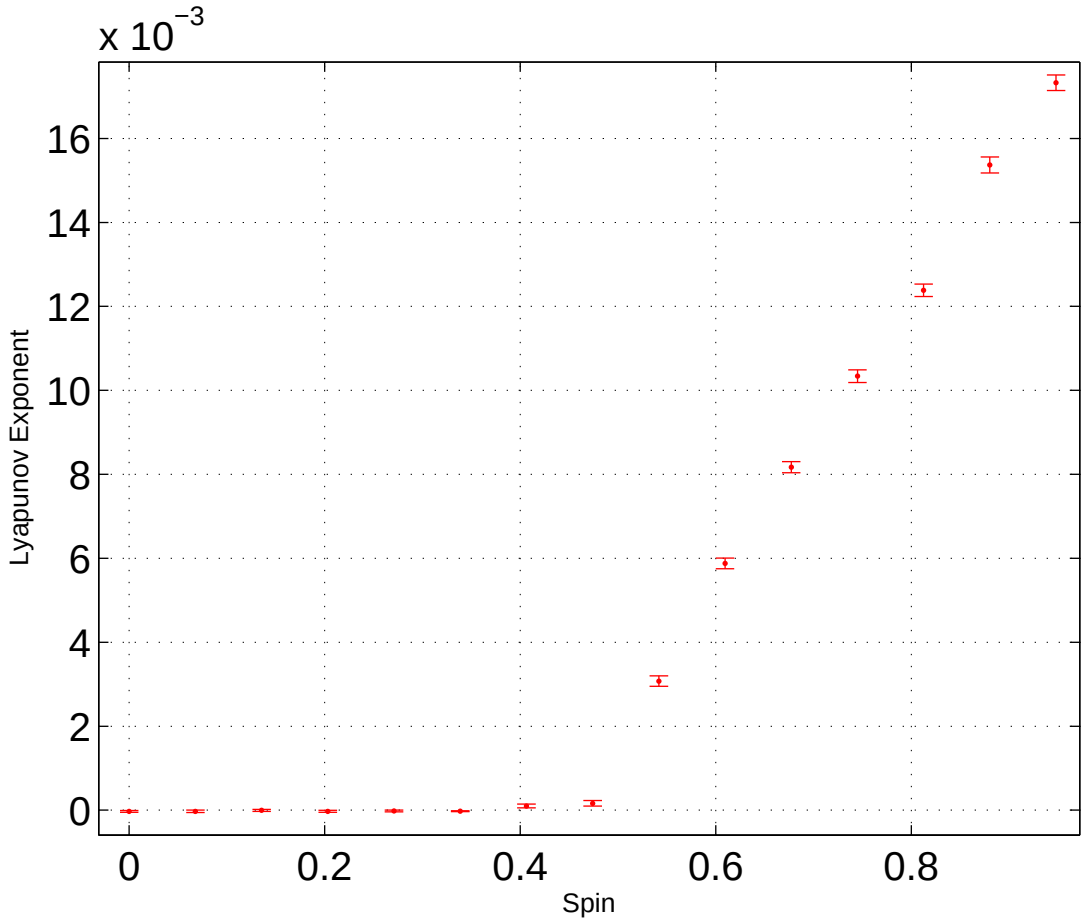

Figure 6.1 These Lyapunov exponent values are given by the constant value in the curve fitting model, eqn. (5.7), with root mean square error bars. The initial spin orientation is $\alpha = 45°$ and $\beta = 90°$. Compare with Fig. 6.2 and Fig. 6.4. Note that orbits seem to become chaotic when the spin becomes close to $S = 0.5$.

We also keep track of the initial conditions in spin that produce these orbits. In

particular we consider what spin magnitudes produce chaotic orbits and how the spin vector's initial orientation affects Lyapunov exponent values. In the first case the spin vector's initial orientation is given by $\alpha = 45°$ and $\beta = 90°$. Here α and β refer to angular coordinates analogous to spherical polar angles ϕ and θ respectively with $\alpha = 0°$ corresponding to the spin vector pointing radially outward from the center of the spacetime and $\beta = 0°$ corresponding to the spin vector pointing up out of the equatorial plane of the spacetime.

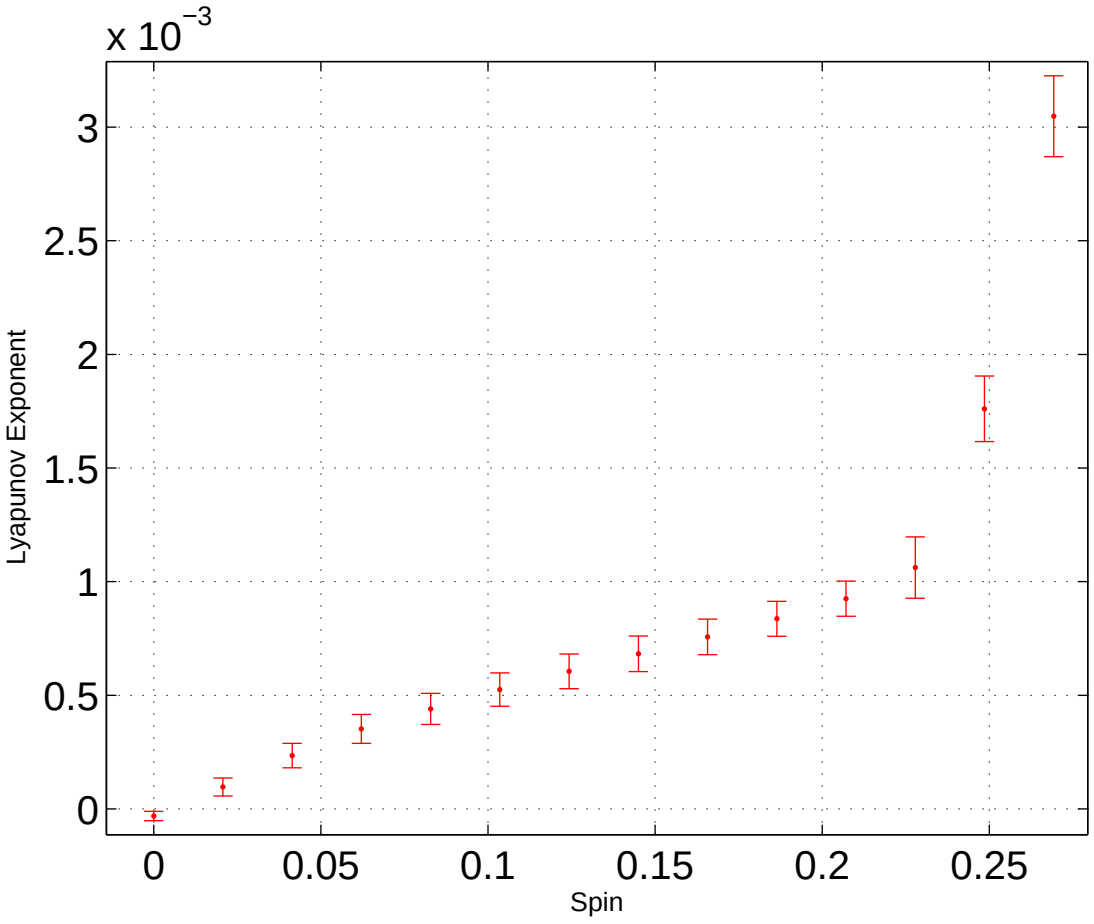

Figure 6.2 These Lyapunov exponent values are given by the constant value in the curve fitting model with root mean square error bars. The initial spin orientation of $\beta = 0°$. All spin values higher than $S = 0.3$ cause the particle to cross the event horizon. Note that lower spin values give exponent values of the same order of magnitude as Fig. 6.1.

As Fig. 6.1 shows, the exponent values for this orbit can be put into one of two groups. From the maximal spin value of 1 down to about $S = 0.5$ there seems to be a well defined trend in the Lyapunov exponent. These exponent values agree with those reported by Suzuki and Hartl; both in the exponent values and how the values change as the spin is changed. From that point on down to zero spin the orbits are not chaotic. In this case we have excellent agreement with the results reported by Suzuki and Hartl.

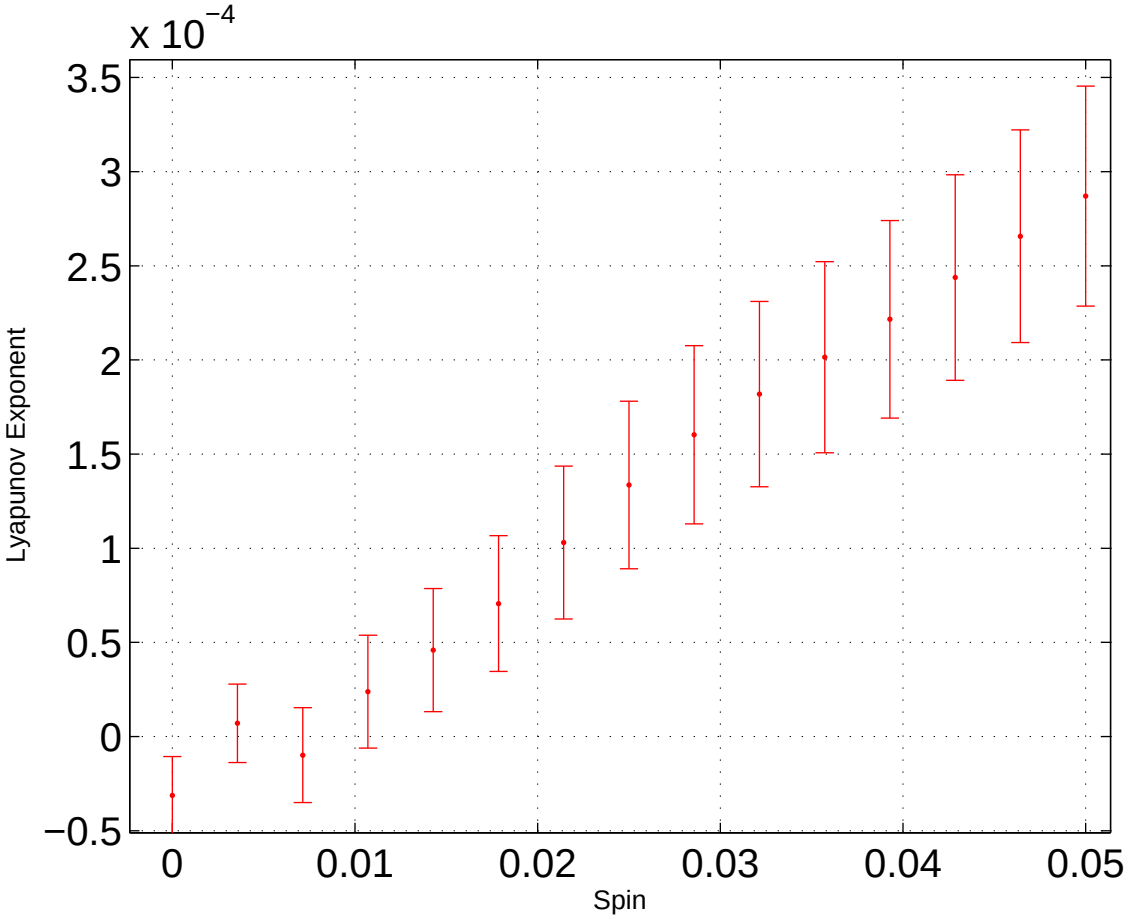

Figure 6.3 These data points are a close up of Fig. 6.2 for small spin values. Notice how zero is outside the error bars for spins as low as $S = 0.015$.

The initial spin vector orientation can also affect the magnitude of the Lyapunov exponent. For example, if we change the spin orientation but otherwise keep the same

initial conditions as before, the particle's behavior changes. When $\beta = 0$, meaning the spin is pointed up perpendicular to the equatorial plane, the spin orbit coupling causes the particle to be pulled in closer to the center of the spacetime. When this interaction becomes strong enough the particle will no longer exhibit a bound orbit, and is captured by the black hole. In Fig. 6.2 we see the Lyapunov exponent values for increasing spin values. Notice that after $S = 0.3$ there is no data. These data points are not included because for $S > 0.3$ the particle is captured.

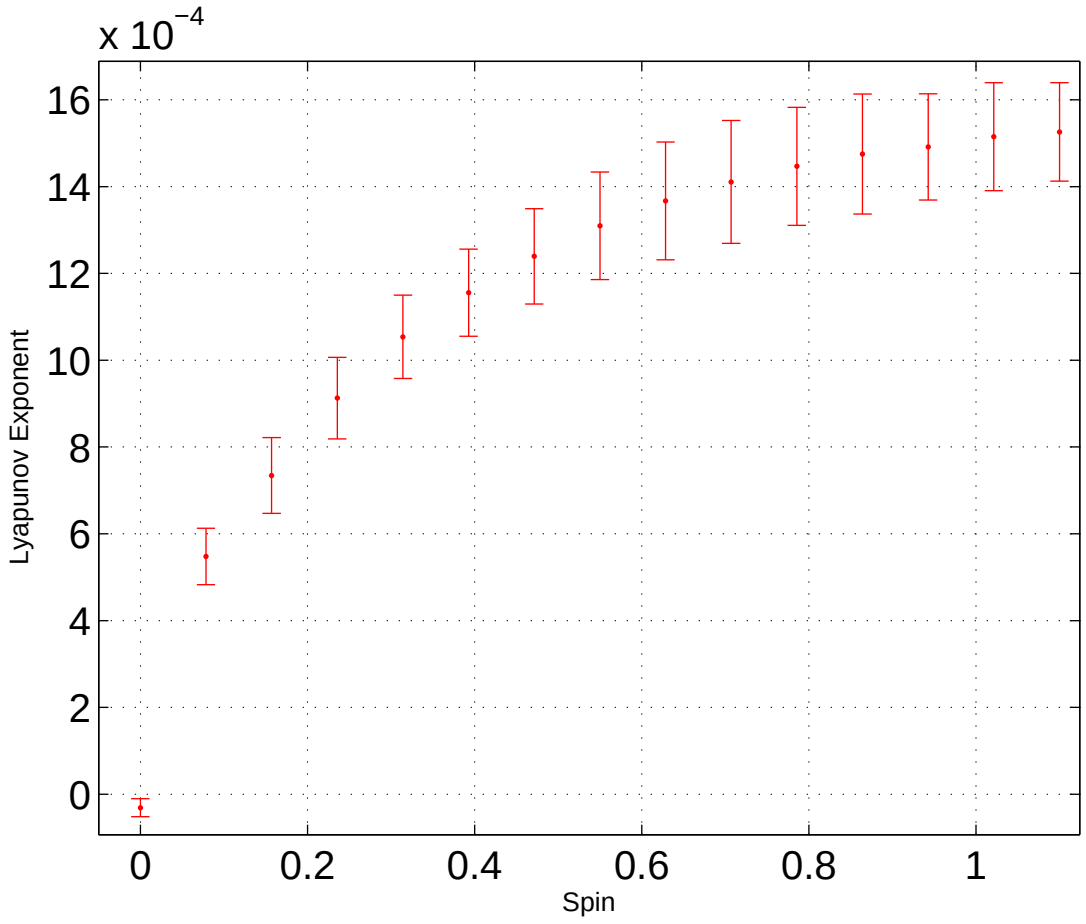

Figure 6.4 These Lyapunov exponents are given by the constant value in the curve fitting model with root mean square error bars. The initial spin orientation is $\beta = 180°$. Note that unlike Fig. 6.1 there is no discontinuity at $S = 0.5$. No large exponent values (compare to Fig. 6.1) appear in this configuration.

Notice also that the exponent values in Fig. 6.2 appear to be nonzero below $S = 0.05$. Since the interaction between the spin angular momentum and the orbital angular momentum pulls the particle in closer, the particle traverses higher curvature regions of the spacetime than the previous case. This spin orientation is the only difference between the two cases. So, by comparing Fig. 6.2 and Fig. 6.4 we can see that the orientation of the spin can have a dramatic effect on the dynamics of the particle.

In Fig. 6.3 we zoom in on the small spin value orbits. This data clearly shows positive Lyapunov exponents for spins as small as $S = 0.015$. This lower bound in spin is far below the bounds given by Suzuki and Hartl. Notice that exponent values in Fig. 6.3 are small in comparison to Fig. 6.1. The method we use to predict the Lyapunov exponent allows us to better distinguish these small exponents from zero. This may be why previous analysis missed these orbits.

When we set the initial spin orientation to $\beta = 180°$, as in Fig. 6.4, the particle is pushed further out from the center instead of pulled closer in. In this case the particle is never captured by the black hole. Instead the particle's orbit stays in areas of the spacetime with slightly less curvature. Also, the Lyapunov exponents stay at the same order of magnitude as the smaller values from Fig. 6.1 for all spin values, but unlike Fig. 6.1 no nonzero spins correspond to a zero exponent. In Fig. 6.5 we look more closely at the small spin values for the same orbit. We notice the continuity in the predicted exponent values, and a nonzero exponent for spin values as low as $S = 0.008$.

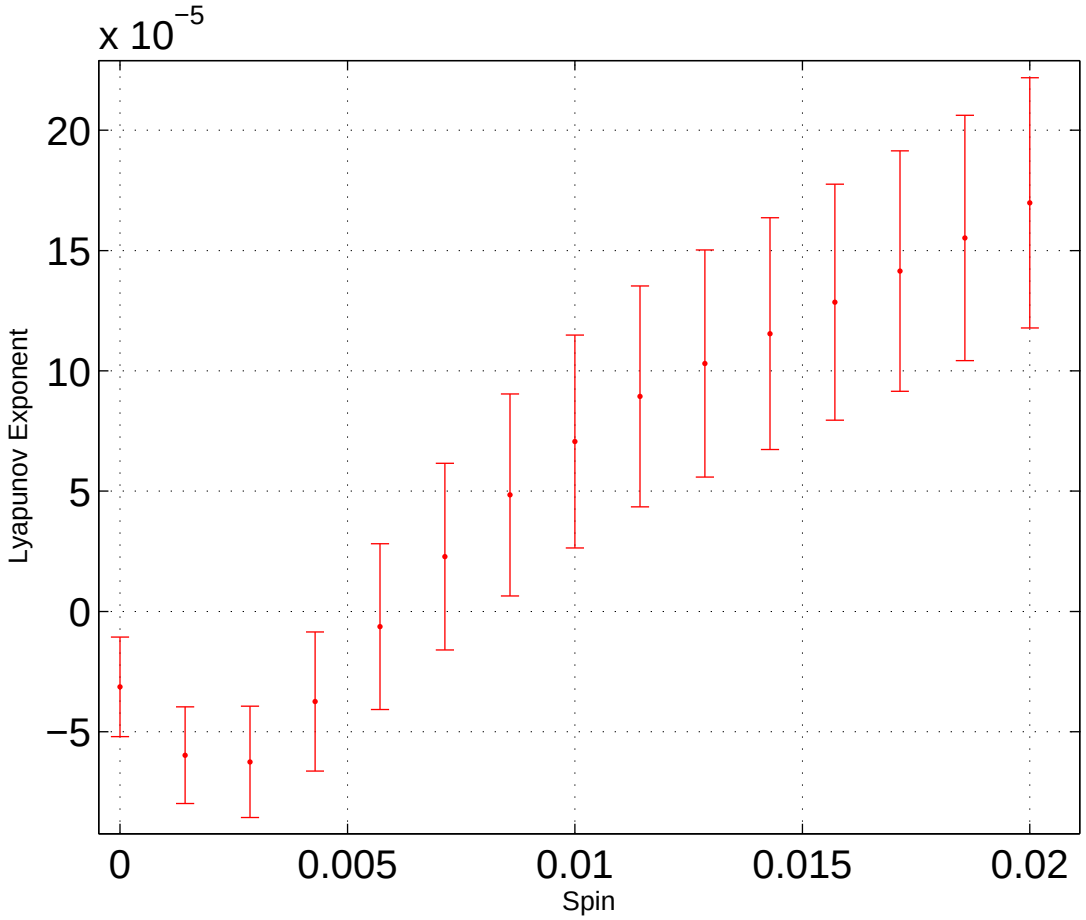

Figure 6.5 These Lyapunov exponents correspond to the small spin case of Fig 6.4. Note the continuous nature to the exponent values and the apparently positive value for spin as low as $S = 0.008$.

6.2 General Orbits

As a type of control group we consider some more general orbits in the Schwarzschild spacetime. We use nearly circular orbits that remain at large radius. This keeps the particle away from high curvature regions of the spacetime. These orbits allow us to check for chaotic effects when curvature is low.

In Fig. 6.6 we see that no positive Lyapunov exponents exist for large radius orbits. In particular these nearly circular orbits stay at about $r = 100m$. This data

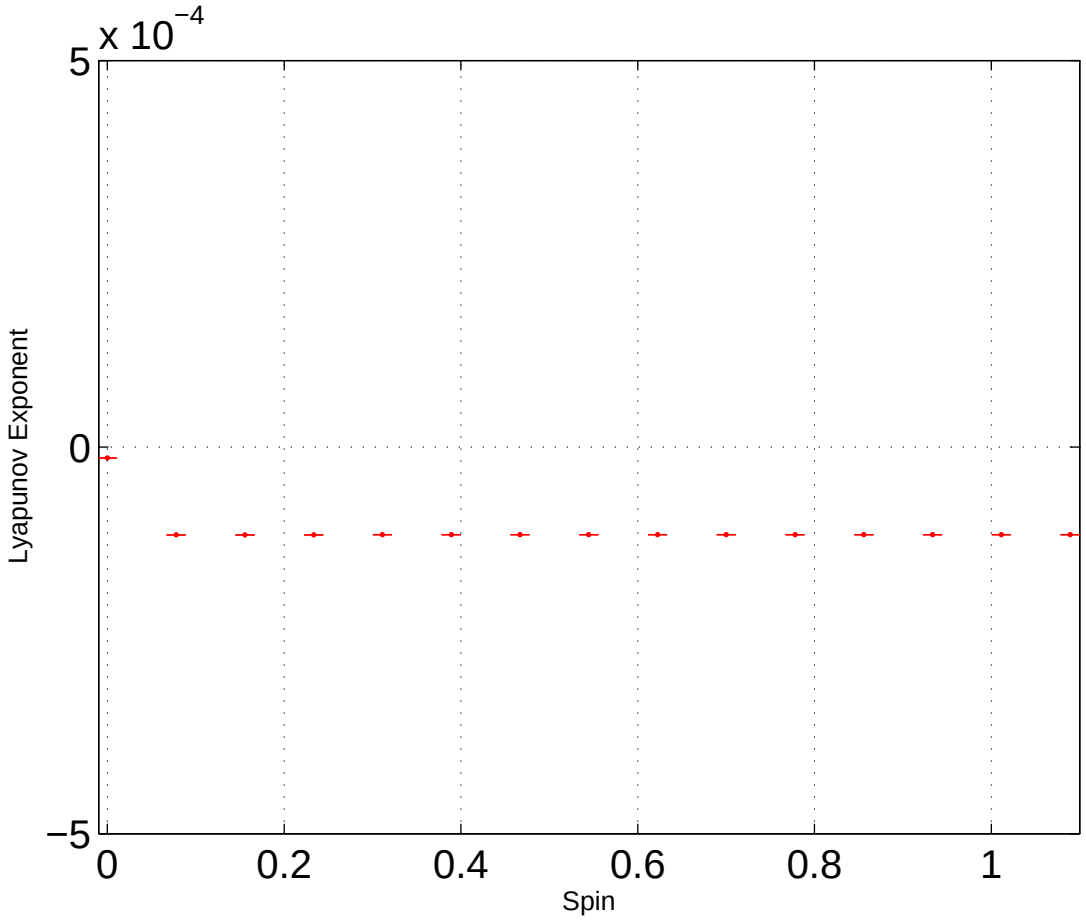

Figure 6.6 These Lyapunov exponents correspond to a nearly circular orbit of radius $r = 100m$. These orbits stay far away from high curvature regions of the spacetime. Note that none are positive, this occurs because the fit 5.7 under shoots the graph of orbits with no chaos.

indicates that for regions of low enough curvature chaotic orbits do not occur.

By reducing the radius of these orbits we find that positive exponent values begin to show up at about $r = 19m$. We then conclude that the interaction between the spin of the particle and the curvature of the spacetime leads to chaotic behavior.

6.3 Knife Edge Orbits

We next consider knife edge orbits. Unlike the orbits we have considered so far, these move through both high and low curvature regions of the spacetime. These orbits start out far from the center of the spacetime, where the curvature is comparatively low. But during the course of their orbits they execute several small orbits in high curvature regions. These types of orbits help us determine whether chaotic orbits must remain in high curvature or just pass through them regularly.

In Fig. 6.7 we have the Lyapunov exponent values for a knife edge orbit that has an outer radius of $r = 100m$ and makes three small radius loops for each large radius orbit. The orientation of the spin is $\beta = 180°$. The angular momentum of the particle is $L = 3.9246$, which is nearly the angular momentum of the particles investigated by Suzuki and Maeda. We choose this spin orientation to keep the particle from being captured by the black hole. Recall that this orientation gives an effective centrifugal force which pushes the particle away from the black hole. This keeps the particle from being captured, but also reduces the number of inner loops traversed in each orbital period. So, the higher the spin value the more the particle retreats from the knife edge.

One important aspect to notice is that the $S = 0$ orbit has a drastically nonzero Lyapunov exponent. This effect is referred to as a "chaos mimic"[1] and Hartl finds the same effect for knife edge orbits in the Kerr spacetime [4]. This effect casts some doubt on the exponent values calculated for the nonzero case. Some confidence is

[1]These chaos mimics have positive Lyapunov exponent due to the dynamics of knife edge orbits. The combination of large and small radius orbits causes $\boldsymbol{\xi}$ to grow very large. Interestingly, these mimics do not occur when we use the geodesic equation as it stands in equation (2.5) as the particle's equations of motion. However, the mimics do show up when the covariant form of the velocity is used. Explicitly, $V^c \nabla_c V_a = 0$.

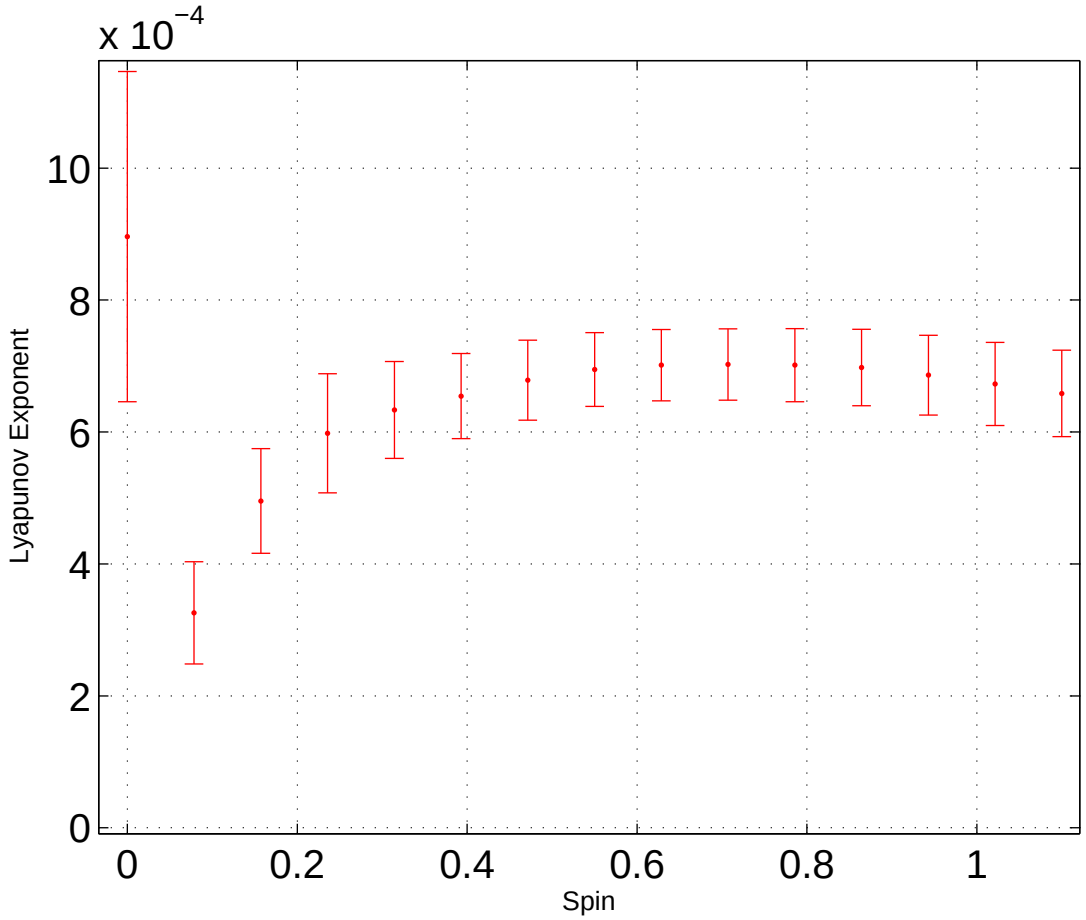

Figure 6.7 These Lyapunov exponents correspond to knife edge orbits. Notice that the $S = 0$ case is very nonzero. This is referred to as a "chaos mimic". The spinless orbit begins at $r = 100m$ and has three inner loops at small radius for each large scale orbit. The initial spin orientation of $\beta = 180°$. In the spinless case $E = 0.997$ and $L = 3.9246$.

restored by the trend in exponent values as spin decreases, explicitly that the values seem to go to zero as spin goes to zero. In Fig. 6.8 we see a close up look at small spin values for the knife edge orbit. We still have the chaos mimic when $S = 0$, but we also see a very clear trend in the exponent values as the spin decreases.

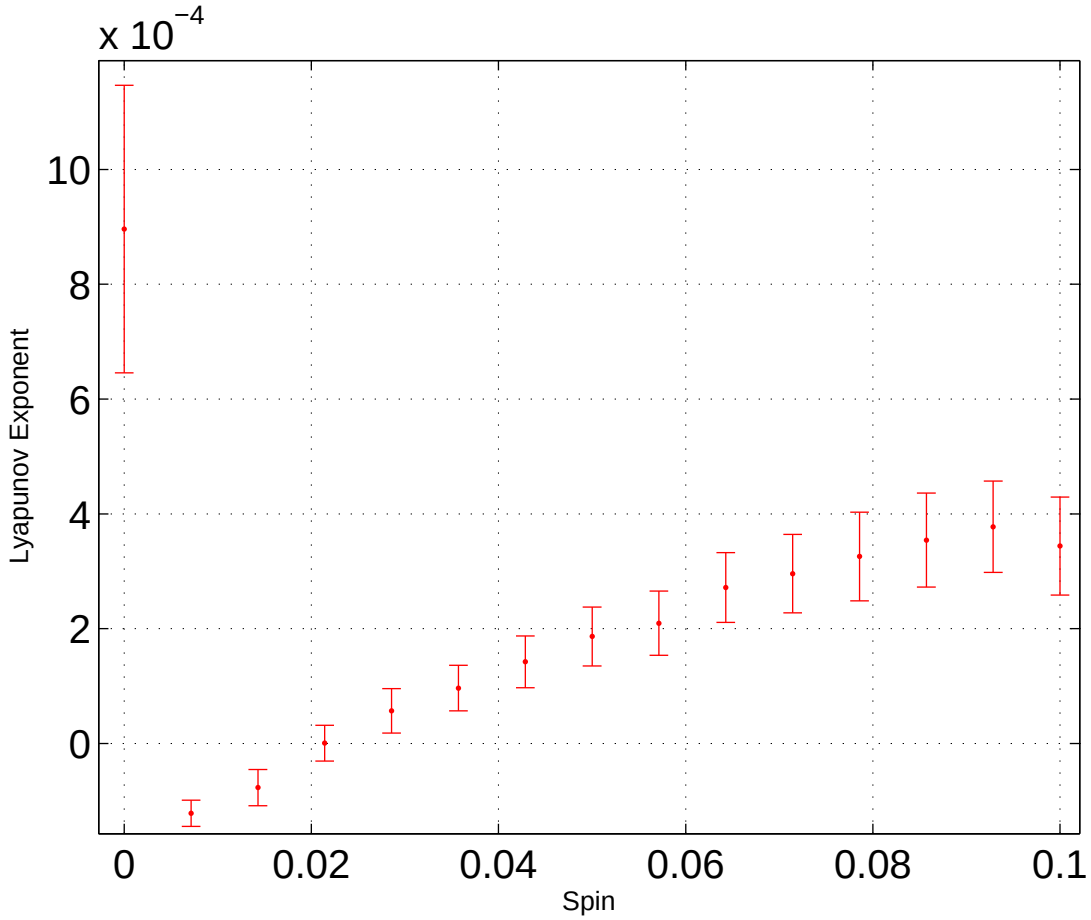

Figure 6.8 These Lyapunov exponents correspond to the same knife edge orbits as Fig. 6.7. Notice that zero is outside the error bars for spin values as low as $S = 0.03$.

6.4 Physical Chaotic Orbit

We now present a particular chaotic orbit with physical spin values. In this case the constants of the motion are $E = 0.9432$ and $L = 3.47$ and the spin vector orientation is $\beta = 0°$. These initial conditions define a knife edge orbit which is constrained to regions of high curvature. The effective potential for this orbit is shown in Fig. 6.9. Notice that the potential well confines the particle with $E^2 = 0.8897$, denoted by the dotted line, to remain close to $r = 6m$.

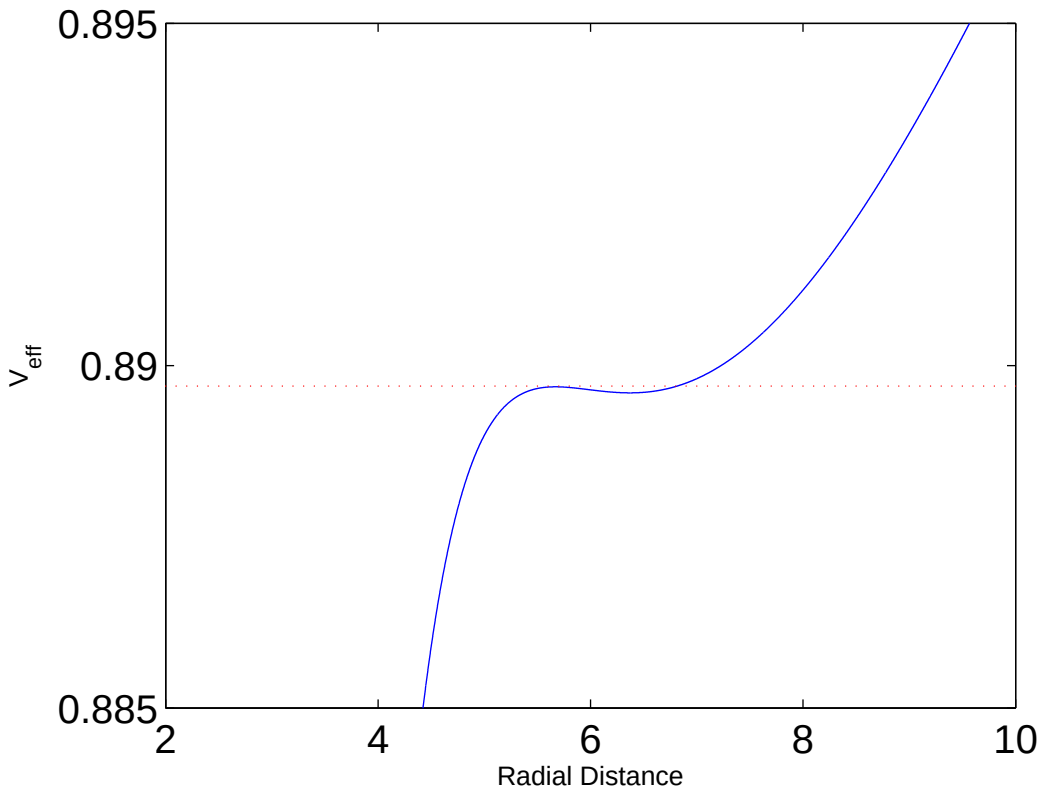

Figure 6.9 The effective potential for corresponding to a knife edge orbit constrained to high curvature regions. This orbits has $L = 3.47$ and $E = 0.9432$. The line $E^2 = 0.8897$ is shown by the dotted line, and shows that the particle is constrained to remain near $r = 6m$.

In Fig. 6.10 we see Lyapunov exponents corresponding to this orbit. Similar to Fig. 6.2 spin values greater than those shown on the graph cause the particle to be captured by the black hole. What is more interesting however, is that these nonzero Lyapunov exponents correspond to physical spin values and that these values have comparable magnitude to the larger exponent values of Fig.6.1.

One concern with this data is that the exponent values seem to converge to the value of the chaos mimic of $S = 0$. We will use the KAM tori corresponding to this orbit to resolve this concern. In figures 6.11 and 6.12 we compare the Poincaré sections of this orbit when $S = 0$ and $S = 3.05 \times 10^{-5}$ respectively. Notice that when

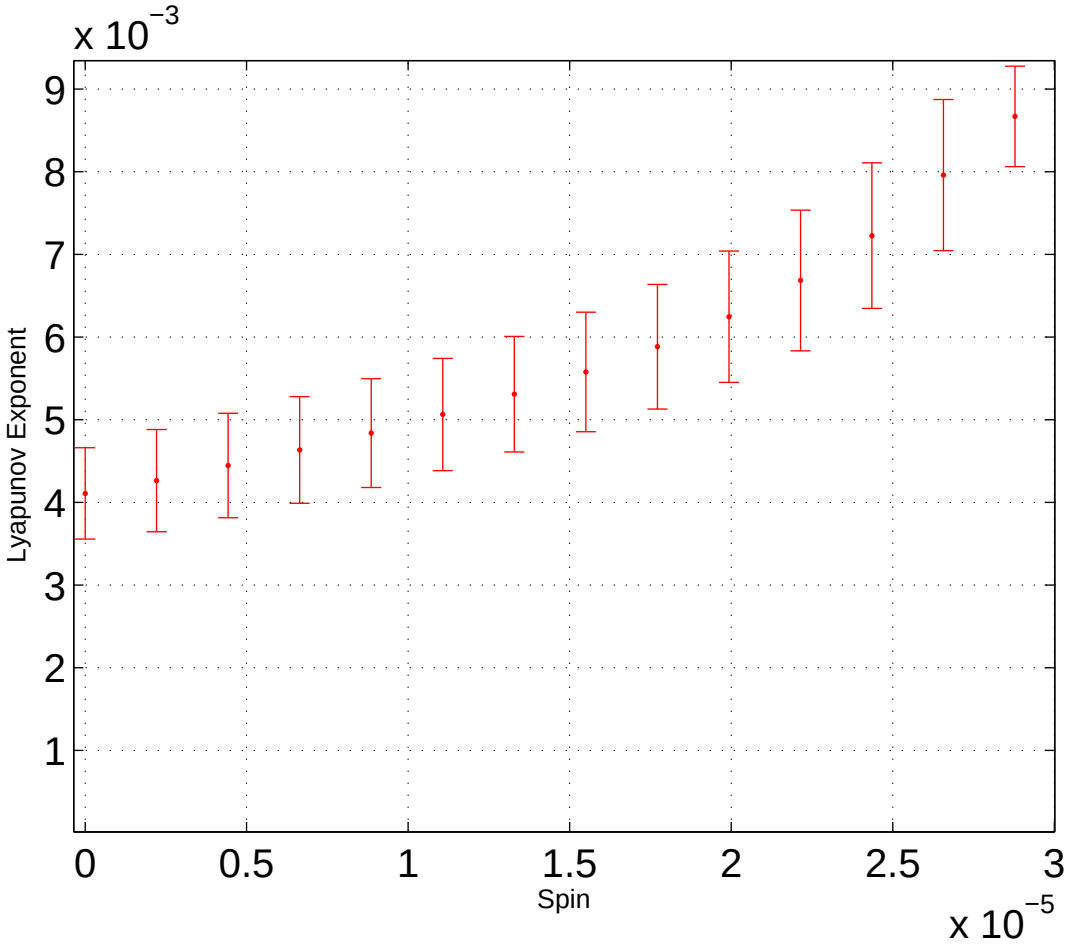

Figure 6.10 Lyapunov exponent values for spin values in the physical range. Note the chaos mimic when $S = 0$ and the magnitude of the exponent is comparable to the larger values of Fig. 6.1.

$S = 0$ the phase space trajectory is confined to the surface of the 2 torus intersected by the $r - P_r$ plane. We can see this detail in the right panel of Fig. 6.11. In the $S = 3.05 \times 10^{-5}$ case the right panel of Fig. 6.12 shows the breaking up of the torus surface described in chapter 4, and is indicative of chaos. Based on the positive indication for chaos given by both the Lyapunov exponent and the Poincaré section we conclude that this orbit is chaotic.

As the spin decreases from $S = 3.05 \times 10^{-5}$ the breaking of the torus becomes smaller and disappears by 2.8×10^{-5}. So, it seems that most of the points of Fig. 6.10

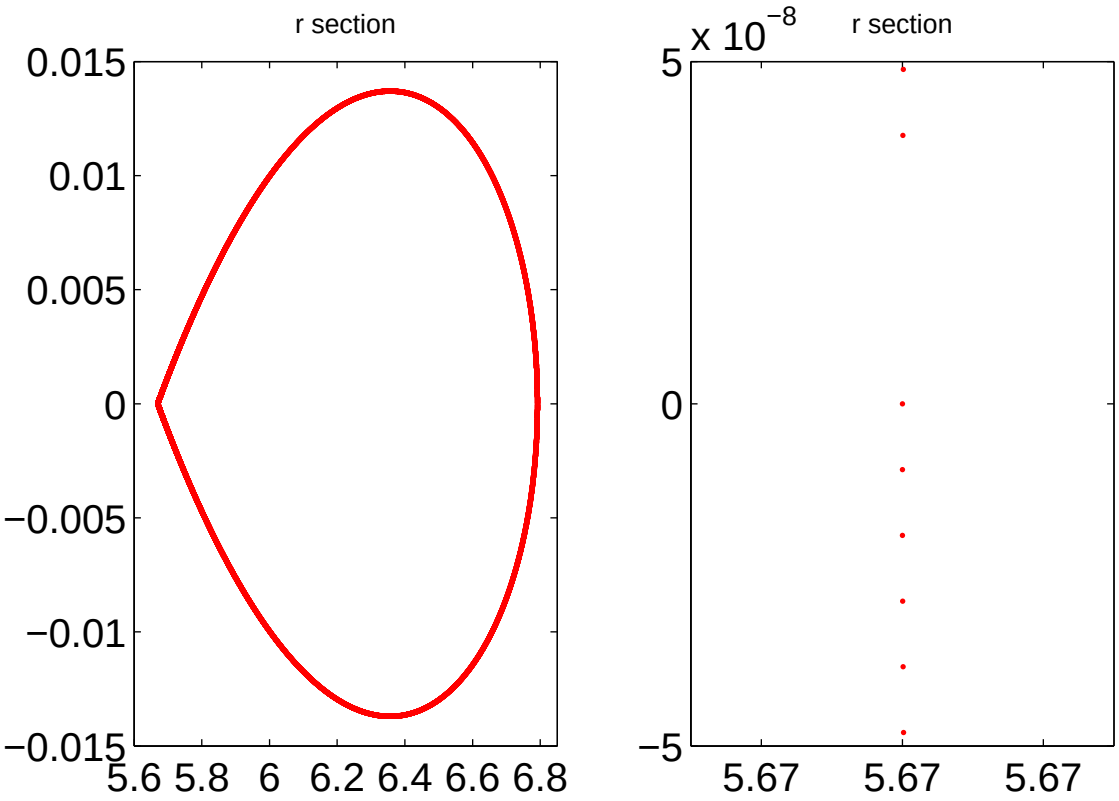

Figure 6.11 Poincaré section in the $r = P_r$ plane when $S = 0$. The right panel shows a close up of the torus edge when r is minimum. Note that each point is constrained to the torus. This implies that the orbit is not chaotic. Compare to the broken torus in Fig. 6.12.

are not truly chaotic. Since these first points seem to converge to the chaos mimic of the $S = 0$ case it is likely that the positive exponent values corresponding to unbroken tori are inflated by the chaos mimic exactly like the zero spin case. We notice from the graph that the final point has smaller error bars than the previous points. Since this orbit is shown to be chaotic by its Poincaré section, the true chaotic behavior of the particle may push it above the exponent magnitude created by the chaos mimic.

We then vary the initial orientation of the spin vector. When $\beta = 180°$ the $S = 0$ exponent remains the same but the larger spin exponents behave much differently than 6.8. Instead increasing in magnitude from the zero spin case the $\beta = 180°$ orbits

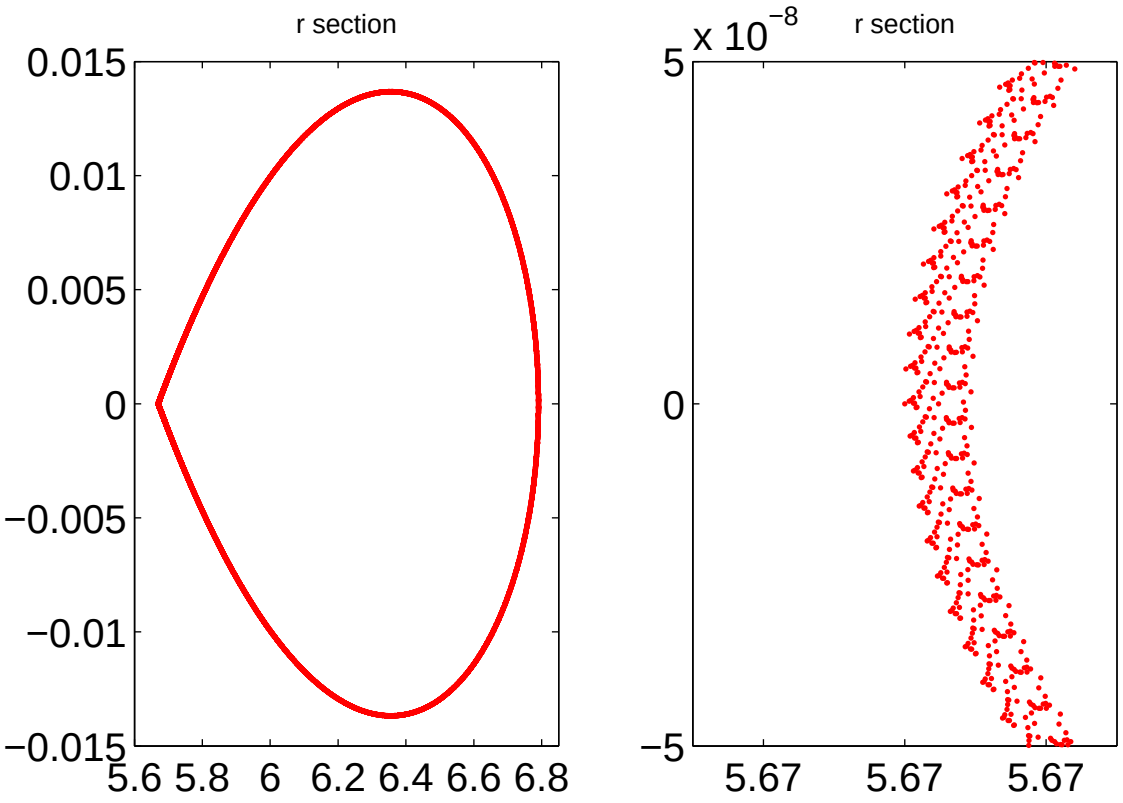

Figure 6.12 Poincaré section in the $r = P_r$ plane when $S = 3.05 \times 10^{-5}$. The right panel shows a close up of the torus edge when r is minimum. Note that the surface of the torus is broken. This implies that the orbit is chaotic. Compare to Fig. 6.11.

decrease in magnitude down to zero. When we make Poincaré sections for these orbits we find that the tori are unbroken, similar to Fig. 6.11. This seems to imply that positive Lyapunov exponents are due to the chaos mimic and not to true chaos.

These mimics only seems to affect the Lyapunov exponent for very low spin values. In the $\beta = 180°$ case mentioned above the exponent values start out at 4×10^{-3} when $S = 0$ but drop down to a constat zero value by $S = 3 \times 10^{-5}$. It seems that the increasing spin values start to prevent chaos mimics at very low spin values. This adds more confidence to the exponent values found for large radius knife edge orbits like Fig. 6.8.

When $\beta = 90°$ the exponents grow in magnitude from the zero case, but not as quickly. This means that the particle is not captured by the black hole for spin values as large $S = 1 \times 10^{-4}$. These orbits also have unbroken phase space tori. Recalling the increase in Lyapunov exponent magnitude in Fig. 6.2 it seems that orbits which are near, in initial conditions, to trajectories that end in the black hole are more chaotic than orbits with similar spin magnitude but otherwise different initial conditions.

Chapter 7

Conclusions

We find that chaotic orbits with physical spin values do exist in the Schwarszchild spacetime. In particular we have shown that for $S = 3.05 \times 10^{-5}$ both the Lyapunov exponent and the Poincaré section indicate a chaotic orbit. These orbits combine the dynamics of knife edge orbits with the high curvature close to the center of the spacetime. While this is a special class of orbit, many decaying orbits may exhibit this behavior before they are captured by the black hole.

The results of our analysis also put the cutoff spin value for chaotic orbits much lower than previously thought for more general obits. Suzuki and Maeda gave a cutoff value of about $S = 0.63$ when the orbital angular momentum of the particle is $L = 4$. The orbits in high curvature that we check have $L = 3.6$ which Suzuki and Maeda claim have no chaotic orbits for any value of spin. We have shown chaotic orbits with zero outside the error bars for spin values lower than $S = 0.008$. The behavior of the exponent values below $S = 0.008$ also suggest that some of these orbits may be chaotic as well. Further investigation of these very small spin orbits need additional analysis to determine whether or not they are truly chaotic.

We have also shown that the initial orientation of the spin affects the dynamics of

the system, but doesn't seem to directly contribute to chaos. Comparing Fig. 6.2 and Fig. 6.4 we see that the orientation of β changes the effect of the spin orbit coupling, either pulling the orbit in closer or pushing it out. The interaction between the spin angular momentum and the orbital angular momentum can also affect whether or not a particle is captured by the black hole. Orbits on the verge of capture trajectories seem to have higher Lyapunov exponents, so this boundary may also give rise to physical orbits with chaotic behavior.

The underlying cause of chaotic behavior seems to be the curvature of the space-time the particle travels through. When the curvature is large enough the spin effects lead to chaotic orbits, but orbits confined to low curvature appear to never be chaotic. We found that when the orbit is within $r = 19m$ positive Lyapunov exponents begin to appear for $0 \leq S \leq 1$. The knife edge orbits show that a particle does not need to remain in these high curvature regions to have a chaotic orbit, but must at least pass through such regions.

Both Suzuki and Hartl claim that more orbits with low spin are chaotic in the Kerr than in the Schwarzschild spacetime. While the Kerr spacetime almost certainly has physical chaotic orbits similar to those in Schwarschild, we suspect that many very low non-zero spins give rise to chaos for more general orbits. Since Hartl found a lower bound for chaotic spin values of about $S = 0.1$, this may also extend into regions of physical spin values. If, for example, this lower bound were reduced by the same factor that Suzuki's bound has been reduced then the Kerr spacetime could have chaotic orbits with $S = 0.0012$. This is quite close to 10^{-4}, the larger edge of physical spin values.

As Hartl points out in [3], in general the direction of greatest stretching of the phase space is nonzero in all the phase space directions defined by the coordinates and momenta. This implies that gravitational waves emitted by binary systems with large

mass ratios could be chaotic. Analyzing these systems for gravitational wave emission would then be important for creating more accurate gravitational wave detection filters.

It is also possible that a charged spinning particle may have different orbital dynamics. The equations of motion for a electrically charged spinning particle in a given spacetime with an electromagnetic field were found by Souriau. [17] They are :

$$V^c \nabla_c P^a = -\frac{1}{2} R^a{}_{bcd} V^b S^{cd} + q F^a{}_b V^b - \frac{1}{2} \lambda S^{bd} \nabla^a F_{bd} \tag{7.1}$$

$$V^c \nabla_c S^{ab} = P^a V^b - P^b V^a + \lambda \left[S^{ad} F_d{}^b - S^{bd} F_d{}^a \right] \tag{7.2}$$

where q is the charge of the spinning particle and λ is an electromagnetic coupling scalar. These equations are obviously more complicated than the uncharged case, but whether they would significantly effect how chaotic an orbit might be remains an open question. It would be especially important to consider realistic values of charge for both the black hole and the orbiting particle.

At the time of completion we found a small error in the derivation of the Jacobian Matrix. We are currently fixing the problem to be sure that it does not affect our results greatly. We feel confident in our results in that they replicate much of the work done by Suzuki and Hartl. Also, the physical chaotic orbit is not affected by this error since KAM tori are unaffected by the Jacobian.

Bibliography

[1] J. Levin and G. Perez-Giz, "A Periodic Table for Black Hole Orbits," Phys. Rev. D 77 (2008).

[2] S. Suzuki and K. Maeda, "Chaos in Schwarzschild spacetime: The motion of a spinning particle," Phys. Rev. D **55,** 4848–4859 (1996).

[3] M. D. Hartl, "Dynamics of spinning test particles in Kerr spacetime," Phys. Rev. D 67 (2003).

[4] M. D. Hartl, "Survey of spinning test particle orbits in Kerr spacetime," Phys. Rev. D 67 (2003).

[5] J. Levin, "Gravity Waves, Chaos, and Spinning Compact Binaries," Phys. Rev. Lett. **84,** 3515–3518 (2000).

[6] N. J. Cornish, "Comment on "Gravity Waves, Chaos, and Spinning Compact Binaries"," Phys. Rev. Lett. **85,** 3980–3980 (2000).

[7] S. A. Hughes, "Comment on "Gravity Waves, Chaos, and Spinning Compact Binaries"," Phys. Rev. Lett. **85,** 5480–5480 (2000).

[8] A. Einstein, in *The Collected Papers of Albert Einstein*, A. J. K. . M. J. K. . R. Schulmann, ed., (Princeton University Press, 1997), No. 30.

[9] R. C. Hilborn, *Chaos and Nonlinear Dynamics*, 2nd ed. (Oxford University Press, 2000).

[10] E. Ott, *Chaos in Dynamical Systems*, 2nd ed. (Cambridge University Press, 2002).

[11] A. Papapetrou, "Spinning test-particles in general relativity," Proc. Roy. Soc. **209,** 248–258 (1951).

[12] W. G. Dixon, "A Covarient Mutipole Formalism for Extended Test Bodies in General Relativity," Nuovo Cim. **34,** 317–339 (1964).

[13] K. Ehlers and E. Rudolph, "Dynamics of Extended Bodies in General Relativity," Gen. Rel. Grav. **8,** 197–217 (1977).

[14] W. G. Dixon, "Dynamics of extended bodies in general relativity I.," Proc. Roy. Soc. Lond. **314,** 499–527 (1970).

[15] O. Semerák, "Spinning test particles in a Kerr field - I," Mon. Not. R. Astron. Soc. **308,** 863–875 (1999).

[16] J. Eckmann and D. Ruelle, "Ergodic theory of chaos and strange attractors," Rev. Mod. Phys. **57,** 617–656 (1985).

[17] J. Souriau, "Modèle de particule à spin dans le champ électromagnétique et gravitationnel," Ann. Inst. Henri Poincaré **20,** 315–364 (1974).

Appendix A

Definitions and Conventions

Unless otherwise specified we use relativistic units defined by $c = G = 1$ where c is the speed of light in vacuum and G is Newton's gravitational constant.

Also, when discussing the different space time geometries in chapter 2 we use a signature of -2 and this corresponds to our orbital modeling. However, when we begin modeling a spinning particle we move to the $+2$ signature.

Our convention for the definition of the Riemann tensor is

$$R^a_{bcd} = \partial_c \Gamma^a_{bd} - \partial_d \Gamma^a_{bc} + \Gamma^e_{bd}\Gamma^a_{ec} - \Gamma^e_{bc}\Gamma^a_{ed} \tag{A.1}$$

and our convention for the Levi-Civita tensor density $\varepsilon_{abcd} = \sqrt{-g}[abcd]$ where $[abcd]$ is the completely antisymmetric symbol.

In numerical simulations the mass of the central object is set to 1. Differential equations were usually solved using a Adams-Bashforth-Moulton routine in Matlab, specifically ode113. We also made some checks on this solver with a Runge-Kutta solver, ode45. In both cases the maximum step size was limited to 1 and the relative tolerance of the integrator was set to 10^{-13}.

Appendix B

Proofs

In this appendix we take P^a to be the momentum vector and S^{ab} to be the antisymmetric spin tensor for a spinning test particle.

B.1 Constants of Spinning Particle Motion

First, we show that for a Killing vector X^a, $C = X^b P_b - \frac{1}{2} S^{bc} \nabla_c X_b$ is a constant of motion.

We will use an identity for Killing vectors and the Riemann tensor,

$$\nabla_c \nabla_b X_a = R_{abcd} X^d \tag{B.1}$$

and recall from Chapter 2,

$$\nabla_a X_b + \nabla_b X_a = 0 \, . \tag{B.2}$$

We also use the equations of motion:

$$V^c \nabla_c P^a = -\frac{1}{2} R^a{}_{bcd} V^b S^{cd} \tag{B.3}$$

$$V^c \nabla_c S^{ab} = P^a V^b - P^b V^a \, . \tag{B.4}$$

Now, to be a constant of motion $V^a\nabla_a C = 0$. So,

$$V^a\nabla_a\left(X^bP_b - \frac{1}{2}S^{bc}\nabla_c X_b\right) = V^a\nabla_a\left(X^bP_b\right) - \frac{1}{2}V^a\nabla_a\left(S^{bc}\nabla_c X_b\right) \tag{B.5}$$

$$= V^aP_b\nabla_a X^b + V^aX^b\nabla_a P_b - \frac{1}{2}V^aS^{bc}\nabla_a\nabla_c X_b - \frac{1}{2}V^a\nabla_c\left(X_b\right)\nabla_a\left(S^{bs}\right). \tag{B.6}$$

Then using (B.1), (B.3), and (B.4),

$$= V^aP_b\nabla_a X^b - \frac{1}{2}X^bR_{bcde}V^cS^{de} - \frac{1}{2}V^aS^{bc}R_{bcad}X^d - \frac{1}{2}\nabla_c\left(X_b\right)\left(P^cV^c - P^cV^b\right) \tag{B.7}$$

$$= V^aP_b\nabla_a X^b - \frac{1}{2}X^bR_{bcde}V^cS^{de} + \frac{1}{2}X^dR_{dabc}V^aS^{bc} - \frac{1}{2}P^bV^c\nabla_c X_b + \frac{1}{2}P^cV^b\nabla_c X_b \tag{B.8}$$

$$= \frac{1}{2}V^aP^b\nabla_a X_b - \frac{1}{2}P^cV^b\nabla_c X_b\,. \tag{B.9}$$

Finally, using (B.2),

$$= \frac{1}{2}V^aP^b\nabla_a X_b - \frac{1}{2}P^cV^b\nabla_b X_c = 0\,. \tag{B.10}$$

Thus, $V^a\nabla_a C = 0$, and C must be a constant of the particle motion.

B.2 Linear Dependence in Spin Tensor

The linear dependence of the spin tensor components is a direct consequence of the supplementary condition:

$$P_aS^{ab} = 0 = P_tS^{tb} + P_rS^{rb} + P_\theta S^{\theta b} + P_\phi S^{\phi b}\,. \tag{B.11}$$

This is really the four equations:

$$P_r S^{rt} + P_\theta S^{\theta t} + P_\phi S^{\phi t} = 0 \tag{B.12}$$

$$P_t S^{tr} + P_\theta S^{\theta r} + P_\phi S^{\phi r} = 0 \tag{B.13}$$

$$P_t S^{t\theta} + P_r S^{r\theta} + P_\phi S^{\phi\theta} = 0 \tag{B.14}$$

$$P_t S^{t\phi} + P_r S^{r\phi} + P_\theta S^{\theta\phi} = 0\ . \tag{B.15}$$

Now, since we take $P^a P_a = -1$ only three of the components of the momentum vector are linearly independent. Without loss of generality we take P_r, P_θ, and P_ϕ to be the linearly independent components of P_a.

This then implies that from (B.13) that

$$S^{rt} = S^{t\theta} = S^{t\phi} = 0 \tag{B.16}$$

which reduces the six nonzero components of S^{ab} to three.

Since the spin tensor has only three nonzero components we may reformulate in terms of a the four vector S_a. Note also that since $S^a S_a = S^2$ is constant, there are only three linearly independent terms in the spin vector, which agrees with our proof.

Index